NRL Memorandum Report 4768

DARPA-NRL Laser Program Annual Technical Report to Defense Advanced Research Projects Agency

1 October 1979 - 30 September 1980

R. BURNHAM, L. F. CHAMPAGNE, R. S. F. CHANG, R. W. WAYNANT, L. J. PALUMBO, AND N. DJEU

Laser Physics Branch
Optical Sciences Division

March 11, 1982

NAVAL RESEARCH LABORATORY
Washington, D.C.

SECURITY CLASSIFICATION OF THIS PAGE (When Data Entered)

REPORT DOCUMENTATION PAGE		READ INSTRUCTIONS BEFORE COMPLETING FORM
1. REPORT NUMBER NRL Memorandum Report 4768	2. GOVT ACCESSION NO.	3. RECIPIENT'S CATALOG NUMBER
4. TITLE (and Subtitle) DARPA-NRL LASER PROGRAM ANNUAL TECHNICAL REPORT TO DEFENSE ADVANCED RESEARCH PROJECTS AGENCY 1 OCTOBER 1979 – 30 SEPTEMBER 1980		5. TYPE OF REPORT & PERIOD COVERED Annual report 1 Oct. 1979 – 30 Sept. 1980 6. PERFORMING ORG. REPORT NUMBER
7. AUTHOR(s) R. Burnham, L.F. Champagne, R.S.F. Chang, R.W. Waynant, L.J. Palumbo, and N. Djeu		8. CONTRACT OR GRANT NUMBER(s)
9. PERFORMING ORGANIZATION NAME AND ADDRESS Naval Research Laboratory Washington, DC 20375		10. PROGRAM ELEMENT, PROJECT, TASK AREA & WORK UNIT NUMBERS DARPA Order 2062; Project 9E20; 65-1164-0-0
11. CONTROLLING OFFICE NAME AND ADDRESS Defense Advanced Research Projects Agency Arlington, VA 22209		12. REPORT DATE March 11, 1982 13. NUMBER OF PAGES 79
14. MONITORING AGENCY NAME & ADDRESS(if different from Controlling Office)		15. SECURITY CLASS. (of this report) UNCLASSIFIED 15a. DECLASSIFICATION/DOWNGRADING SCHEDULE

16. DISTRIBUTION STATEMENT (of this Report)

Approved for public release; distribution unlimited.

17. DISTRIBUTION STATEMENT (of the abstract entered in Block 20, if different from Report)

18. SUPPLEMENTARY NOTES

15A/Sq.cm 2X10 to the -10th power cc/sec)

19. KEY WORDS (Continue on reverse side if necessary and identify by block number)

Lasers
Electrical laser
Laser diagnostics
Electronic state lasers
Chemical kinetics
Electronic state lifetimes
Energy transfer

20. ABSTRACT (Continue on reverse side if necessary and identify by block number)

The e-beam pumped XeCl laser has been investigated experimentally at pump current densities up to ~~150 amp~~ cm^{-2}. The results have been compared with NRL's XeCl laser kinetics code, and satisfactory agreement was found. To obtain a better understanding of the neutral formation channel of XeCl*, the $Xe(^3P_2^1) + HCl$ ($v = 1$) reaction has been studied and a lower bound on the formation rate constant of 2×10^{-10} cm^3 sec^{-1} was deduced. To assess the potential of the Pb vapor Raman converter for rep-pulsed operation, measurements of collisional quenching of $Pb(^3P_2^1)$ and $Pb(^3P_1^1)$ by ground state atoms

(Continues)

DD FORM 1 JAN 73 1473 EDITION OF 1 NOV 65 IS OBSOLETE
S/N 0102-014-6601

SECURITY CLASSIFICATION OF THIS PAGE (When Data Entered)

3.2 X 10 to the -13th power cc/sec

2.0X10 to the -13 power cc/sec

SECURITY CLASSIFICATION OF THIS PAGE (When Data Entered)

20. ABSTRACT (Continued)

were carried out, which yielded rate constants of 3.2×10^{-13} cm^3 sec^{-1} and 2.0×10^{-13} cm^3 sec^{-1} respectively.

SECURITY CLASSIFICATION OF THIS PAGE(When Data Entered)

CONTENTS

FOREWORD

The Laser Physics Branch of the Optical Sciences Division, Naval Research Laboratory, Washington, D. C., prepared this annual report on work sponsored by the Defense Advanced Research Projects Agency, DARPA Order 2062. The projects described are also funded by NRL-ONR research funds. Co-authors of the report were R. Burnham, L. F. Champagne, R. S. F. Chang, R. W. Waynant, L. J. Palumbo, and N. Djeu.

FY 80 ANNUAL TECHNICAL REPORT

1.	DARPA Order	2062
2.	Program Code Number	9E20
3.	Name of Contractor	Naval Research Laboratory
4.	Effective Date of Contract	1 October 1979
5.	Contract Expiration Date	30 September 1980
6.	Amount of Contract	$320,000
7.	Contract Number	62301E
8.	Principal Investigator	N. Djeu
9.	Telephone Number	(202) 767-3217
10.	Project Scientist	L. F. Champagne
11.	Telephone Number	(202) 767-2512
12.	Title of Work	DARPA/NRL Laser Technology Program

SPONSORED BY

DEFENSE ADVANCED RESEARCH PROJECTS AGENCY

DARPA Order 2062

SCALING EXPERIMENTS ON THE ELECTRON BEAM PUMPED XeCl LASER

During the past fiscal year experiments, guided by the numerical model, were performed on the electron beam pumped XeCl laser with the hope of improving laser performance. These experiments fell into two catagories; temperature dependent laser performance (A) and laser performance at higher pumping currents (C). Modifications were made to the existing system in order to investigate both the temperature dependence and increased pump current characteristics. The temperature dependent studies increased our knowledge of the XeCl laser and its associated physics but did not result in any improvement in laser performance. Operation at increased current densities required modifications which shortened the optical pulse obtained in previous work from 600 ns to 400 ns. However, peak currents were increased from 7 A-cm^{-2} to 15 A-cm^{-2}.

Briefly, we find that at these higher pumping currents and shorter optical pulse lengths the extracted energy per pulse and intrinsic efficiency increased. This is accomplished by increasing the optical transmission from 70% to 92%. The measured small signal gain increased with increasing pumping current by ~ 15%. But, the background absorption in these laser mixtures measured at t = 300 ns and ~ 15 A-cm^{-2} was comparable to that measured at t = 600 ns and ~ 7 A-cm^{-2}. This increase in small signal gain and also ratio of gain to absorption resulted in increased output power and intrinsic efficiency. Based on the reported work of Mathematical Sciences Northwest[1] (MSNW), argon was substituted for neon as diluent at these higher pumping currents. Calculated intrinsic efficiencies were ~ 5% higher with argon than with neon. The extraction energies were higher in both cases at these higher pumping currents the optimum transmission in both cases was 92%. Comparable energy was extracted from two atmospheres of argon to that obtained in 4 atmospheres of the neon mixture. This increased the extracted energy obtainable in XeCl laser mixtures from ~ 1 J-ℓ^{-1}-atm (Ne) to 2.35 J-ℓ^{-1}-atm^{-1} (Ar).

Manuscript submitted January 18, 1982.

A. Temperature Dependent Studies of the XeCl Laser

At the beginning of FY 80, intrinsic efficiencies of 6.5% had been demonstrated for the electron beam pumped XeCl laser. Laser performance could be improved further if the relatively large transient optical absorption observed in neon/xenon/HCl mixtures (~ 0.25%-cm^{-2}) could be reduced.

The major absorber species in the laser mixture is not the diluent (argon or neon) but rather is an excited state species in xenon, most likely the dimer ion Xe_2^+.[2] Depending on where the peak absorption cross section lies with respect to the XeCl laser wavelength and also on the shape of that absorption profile as a function of temperature, transient absorption by the dimer ion would become less detrimental with either ambient heating or cooling of the laser mixture. However, there was a discrepancy between the observed[3] and predicted[4] absorption profile for Xe_2^+. In addition, laser performance had degraded slightly when the active medium was ambiently heated from 300°K to 450°K. In order to better understand the role of the absorber species and to determine whether XeCl laser performance would improve at lower temperatures the long pulse system was modified to operate down to ambient temperatures of ~ 250°K.

Ambient cooling of the laser mixture did not result in any dramatic improvement in laser performance. Figure 1 plots the small signal gain and background absorption in neon/xenon/HCl mixtures from 260°K to 450°K. The small signal gain decreased with increasing temperature. No change in background absorption in the laser mixture was observed over this temperature range. In marked contrast to room temperature operation, at elevated temperatures, it was necessary to passivate the laser chamber between fills. Measured gain and extracted energy was a sensitive function of wall passivation at temperatures above 350°K. The modest improvement in gain and output power at the lower ambient temperatures is attributed to either more effective wall passivation, removal of impurities or a slight but real increase in the small signal gain. The marginal improvement in laser performance to be gained at lower ambient temperatures (< 10%) does not justify the considerable complexity involved in maintaining a system at these temperatures.

Additional broad band absorption studies were performed in order to define the absorption profile in xenon plasmas and the role of 3s,5p atomic transitions observed in neon plasmas. In xenon plasmas, a dual absorption

band was observed.[5,6] One absorption peak correlated well with the corrected theoretical prediction of Wadt[7] and the predicted profile based on configuration interaction calculations of Michels et al.[8] The second absorption peak, blue shifted from the dimer ion peak was observed at 3050 Å. This second absorption profile is attributed to the excited molecular species Xe_2^*. Both species contribute to absorption at 3080 Å. The formation of the Xe_2^* is a sensitive function of pumping current.[6] It is also assumed to be a sensitive function of time in an analogous way to those Xe_2^* absorber species observed by Arai and Firestone which occur in the near infrared.[9] In pure neon plasmas a large broadband of absorption and several atomic transitions are observed.[6] Small quantities of xenon completely removed these line absorptions and significantly reduced the broad band absorption in the neon plasmas.

B. System modifications

During the past fiscal year modifications were made to the existing long pulse system in order to increase pumping currents incident to the active volume from 7 A-cm^{-2} to ~ 15 A-cm^{-2}. The motivation for going to higher pumping currents is to demonstrate that increased specific energy output can be obtained by increasing the pumping current. Also, it was not clear that the overall laser efficiency would also increase at these higher pumping currents. However, long pulse kinetics experiments in which the fluorescence was observed at 1.5 and 7.0 A-cm^{-2} indicated that formation efficiency increases with pumping current in this current range. This current dependence is qualitatively confirmed by our XeCl laser kinetics code, which predicts a continuation of the trend up to 15 A-cm^{-2}.

To obtain the increased pumping current two modifications were made to the existing system. A peaking circuit was added in order to reduce the risetime of the current pulse. The reduced current risetime permits us to relax the closure constraint and still maintain reliable operation. Also, tantalum emitters were replaced with carbon felt at the gun cathode. With carbon felt as the cathode emitter, the diode impedance does not change significantly during the pump pulse. Voltage droop during the pump pulse is minimal. With these two modifications reliable operation was demonstrated for a closure constraint of 3 cm-μsec^{-1} as compared to the previous value of 4 cm-μsec^{-1}. Peak currents of 16 A-cm^{-2} $\pm$ 2 A-cm^{-2} and average currents of 14 A-cm^{-2} $\pm$ 2 A-cm^{-2} for 200 ns and 12.5 A-cm^{-2} for 400 ns were demonstrated.

Figure 2 is a schematic of the peaking circuit which was retrofitted to the existing system. Without the peaking circuit, the voltage rise was limited by the inductance of the Marx (L_m) and of the diode (L_{diode}),

$$\tau_r = \frac{2L}{R} = \frac{2(1.25 + 0.25)\ \mu H}{15\ \Omega} = 200\ ns, \tag{1}$$

where R is the diode impedance. With the addition of the peaking circuit, the relatively large inductance of the Marx is replaced by the inductance of the peaking circuit plus the associated stripline. The voltage risetime of the system was reduced to 80 ns (10% to 90%) (Fig. 3). The observed decrease in risetime from 200 ns to 80 ns allows us to determine the inductance of the peaking circuit.

$$L_{PC} = \frac{\tau_r' R}{2} - L_{Diode} = \left[\frac{(0.08)\ 15\ \Omega}{2} - 0.25\right] = .35\ \mu H, \tag{2}$$

where τ_r' is the voltage risetime.

Figure 3 plots the shape of the voltage pulse incident to the foil as a function of pressure in the peaking switch. As the peaking switch pressure was increased from 15 psig to 25 psig the voltage droop decreased, as did the risetime.

The energy stored in the peaking circuit is

$$E = 1/2\ cv^2 = 1/2\ (26)(2.75 \times 10^5)^2 = 980\ J, \tag{3}$$

and the power is

$$P = \frac{v^2}{R} = \frac{(2.75 \times 10^5)^2}{15} = 5 \times 10^9\ \text{watts}. \tag{4}$$

The energy supplied by the peaking circuit is

$$\Delta E_{PC} = 1/2\ P\ \tau_r - 1/2\ P\ \tau_r' = 300\ J, \tag{5}$$

so that

$$\frac{\Delta E_{PC}}{E} \simeq .3\ . \tag{6}$$

This indicates that ~ 30% of the energy contained in the peaking capacitors is used. The length of the pump pulse is limited by the physical size of the peaking circuit which in this case is limited by the space available in the existing system.

Figure 4 is a plot of a typical current pulse shape incident to the foil (I_b). The figure illustrates the decreased rise time which occurs when the pressure is increased in the peaking switch.

In addition to contributing to relaxation of the closure constraint, the use of carbon felt as a cathode material in place of the tantalum emitters offers the advantage of increased durability, because the carbon felt configuration is more rugged and therefore, less susceptible to damage and degradation. Previously, damage to the delicate tantalum emitters resulted in steadily degrading current densities during the lifetime of the emitter.

The reliability of operation and the peak current obtained in the present system is limited by the reliability of the diverter switch. Improvements in the design of this switch would increase both the reliability of operation and also peak current density.

C. XeCl laser performance at 15 A-cm^{-2}

Previously, power efficiencies of ~ 6.5% were obtained in XeCl for optical pulses ~ 600 ns for ~ 7 A-cm^{-2} incident to the active volume. However, the energy efficiency (energy extracted divided by the energy deposited) was ~ 5.5%. With the addition of the peaking circuit to the long pulse system, the voltage rise incident to the foil was reduced from ~ 200 ns to ~ 80 ns. Since the 10 W energy electrons (V < 150 kV) do not penetrate the foil the voltage rise time incident to the active volume is ~ 40 ns. In practice this represents a much improved approximation to a square wave pumping pulse and permits the measured energy efficiency to approach the power efficiency. The laser efficiencies quoted in Table 1 are actually calculated energy efficiencies.

In experiments performed at 15 A-cm^{-2} a small increase was calculated in intrinsic efficiency above that previously reported at 7 A-cm^{-2}. The improved efficiency and output power is attributed to increasing the useful power coupled out of the cavity at the higher pumping current. This conclusion is based upon the measured increase in output power when the output coupling was increased for both argon and neon as diluents. In each case,

the extracted energy increased by ~ 15% when the optical transmission was increased from 70% to 92%. The small signal gain and background absorption were also measured with both argon and neon as a diluent. At these higher pumping currents the measured gain increased by ~ 15% but the background absorption did not differ with that previously measured at 7 A-cm^{-2}. Under low pumping current conditions (7 A-cm^{-2}) the small signal gain in neon diluent laser mixtures was observed to be ~ 2.6%-cm^{-1} at t = 600 ns after the start of the pumping pulse.[2] The background absorption was observed to be (0.25 $\pm$ 0.05)%-cm^{-1}. At 15 A-cm^{-2} the small signal gain and absorption, (independent of diluent) was measured to be (3.0 $\pm$ .2)%-cm^{-1} and (0.2 $\pm$ 0.1)%-cm^{-1} respectively. These measurements were obtained at t = 300 ns after the start of the pump pulse.

Table 1 lists energy (in J-ℓ^{-1} and J/ℓ-atm) as well as efficiency for two different pulse lengths. The values quoted here were obtained for an average current density of 13 A-cm^{-2} for t = 200 ns and 11.5 A-cm^{-2} for 400 ns. In the case of neon the energy extracted is comparable to that obtained at lower pump currents (7 A-cm^{-2}) and longer pumping times (600 ns).

The energy extracted and the calculated efficiency in a single pulse was comparable within experimental uncertainty limits for both diluents. However, in the case of argon the total operating pressure was two atmospheres and in neon it was four atmospheres. Consequently, when argon is used as diluent in place of neon the extracted energy in joules per liter atmosphere increased by a factor of two over that obtained in neon.

In these experiments, the current density maintained for a particular pulse length was determined by the capacitance and associated inductance of the particular peaking circuit used in this system.

For a fixed current density incident to the active volume, extracted energy was observed to scale linearly with optical pulse length over a range from 200 ns to 600 ns. It is reasonable to conclude that if a current density of ~ 13 A-cm^{-2} could be maintained for 600 ns then, laser efficiencies ~ 7% would also be maintained over this time period.

References

1. L. A. Levin, S. E. Moody, E. L. Klosterman, J. J. Ewing and R. E. Center, 33rd Annual Gaseous Electronics Conference, Palo Alto, CA, 1977, Paper FB-4.

2. L. F. Champagne, L. J. Palumbo and T. G. Finn, Appl. Phys. Lett. 34, 315 (1979).
3. R. S. F. Chang and L. F. Champagne, Appl. Phys. Lett. 36, 879 (1980).
4. W. R. Wadt, D. C. Cartwright and J. S. Cohen, Appl. Phys. Lett. 31, 672, (1977).
5. L. F. Champagne and R. S. F. Chang, J. De Physique, Tome 41, C9-449 (1980).
6. L. F. Champagne, Atomic Collision Physics, Vol. III, (Academic Press, Inc., New York, 1981), in press.
7. W. R. Wadt, J. Chem. Phys. 73, 3915 (1980).
8. H. H. Michels, R. H. Hobbs and L. A. Wright, J. Chem. Phys. 71, 5053 (1979).
9. S. Arai and R. F. Firestone, J. Chem. Phys. 50, 4574 (1969).

TABLE I

τ_{op}		Argon	Neon
200 ns	Energy (J/ℓ)	2.8	2.45
	Energy (J/ℓ-atm)	1.4	.61
	Efficiency (%)	7.1	6.9
400 ns	Energy (J/ℓ)	4.7	4.1
	Energy (J/ℓ-atm)	2.35	1.05
	Efficiency (%)	6.6	6.3
	Gain (%-cm^{-1})	(3.0 $\pm$ .2)	(3.0 $\pm$ .2)
	Absorption (%-cm^{-1})	0.2 $\pm$ 0.1	0.2 $\pm$ 0.1

Table I gives the characteristics of the electron beam pumped XeCl laser operated at high pump currents (11-13 A-cm^{-2}) for both neon and argon when T=92%.

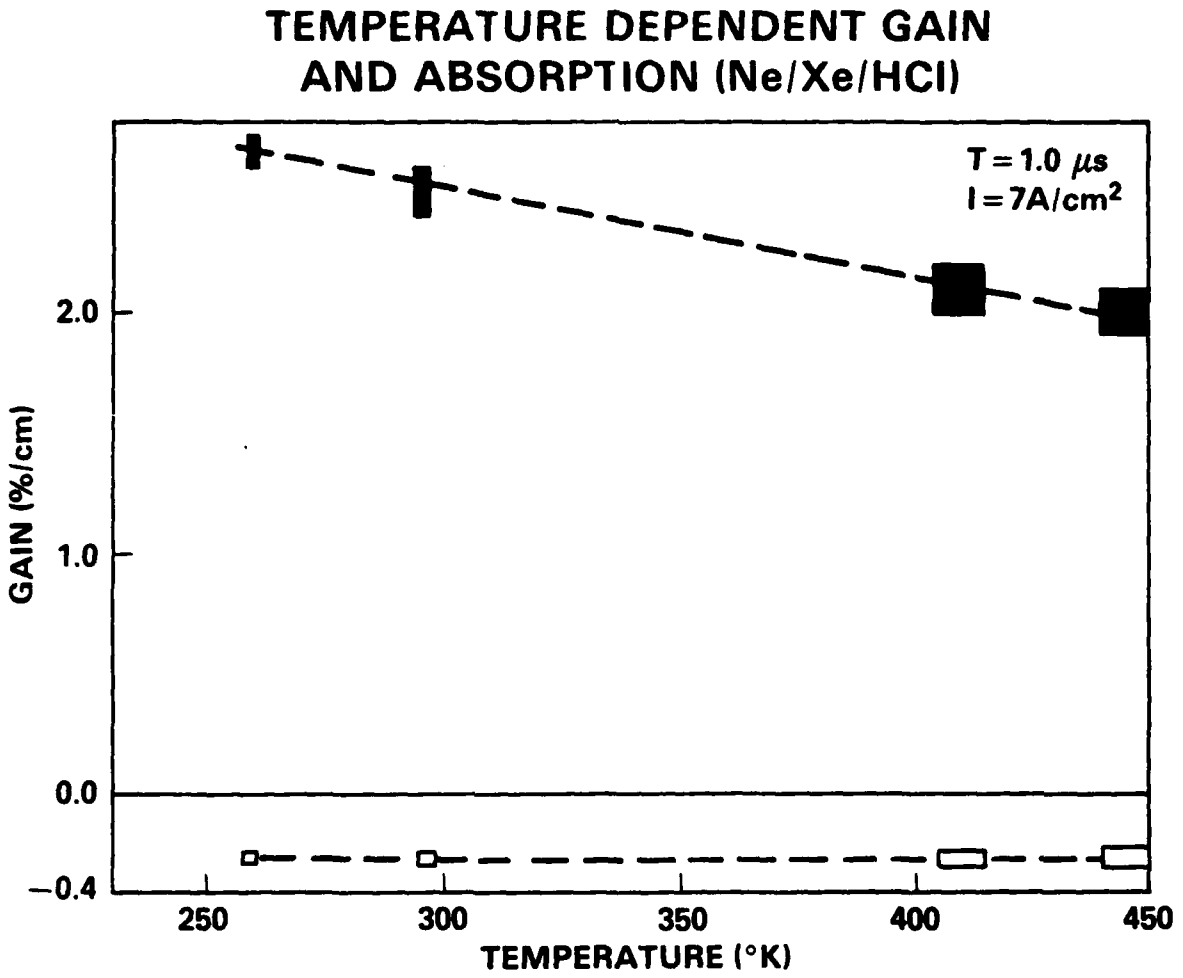

Fig. 1 - Measured small signal gain and background absorption as a function of temperature at 308.0 nm

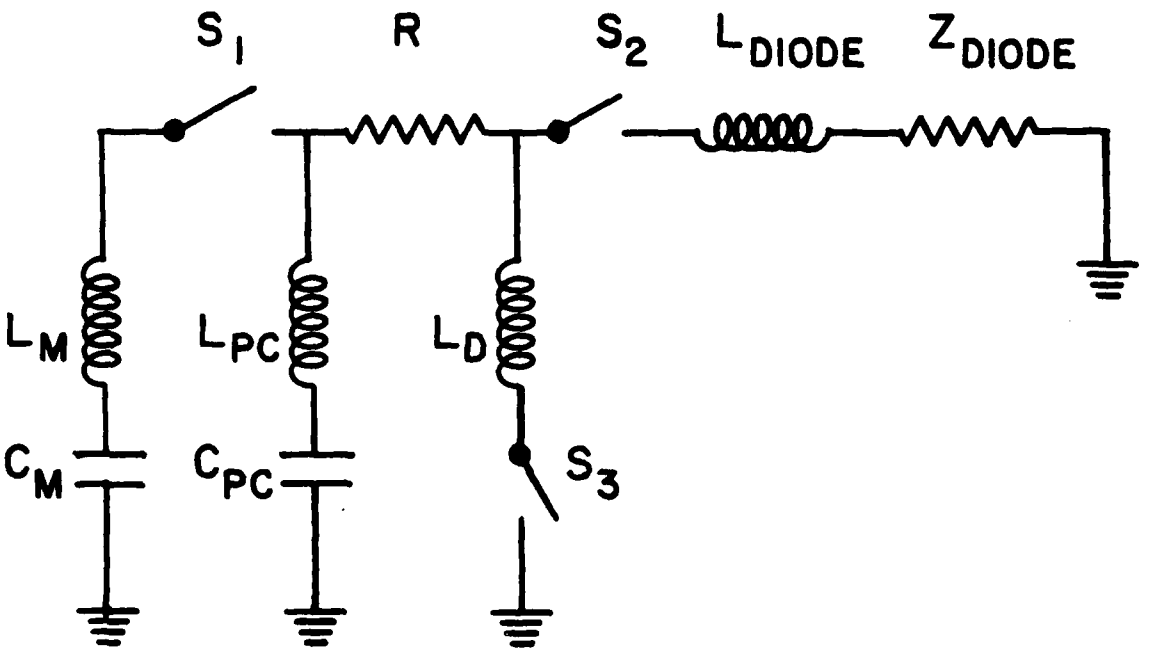

Fig. 2 - Schematic diagram of the electron gun charging circuit showing the inductance of the Marx (L_m), peaking circuit (L_{PC}), diode (L_D) the capacitance of the Marx (C_m) and peaking circuit (C_{PC}) and circuit impedance. The three-key switches: the Marx switch (s_1), the peaking switch (s_2) and the diverter switch (s_3) are also known. The inductance of the diverter switch is donated as L_D.

VOLTAGE CHARACTERISTIC

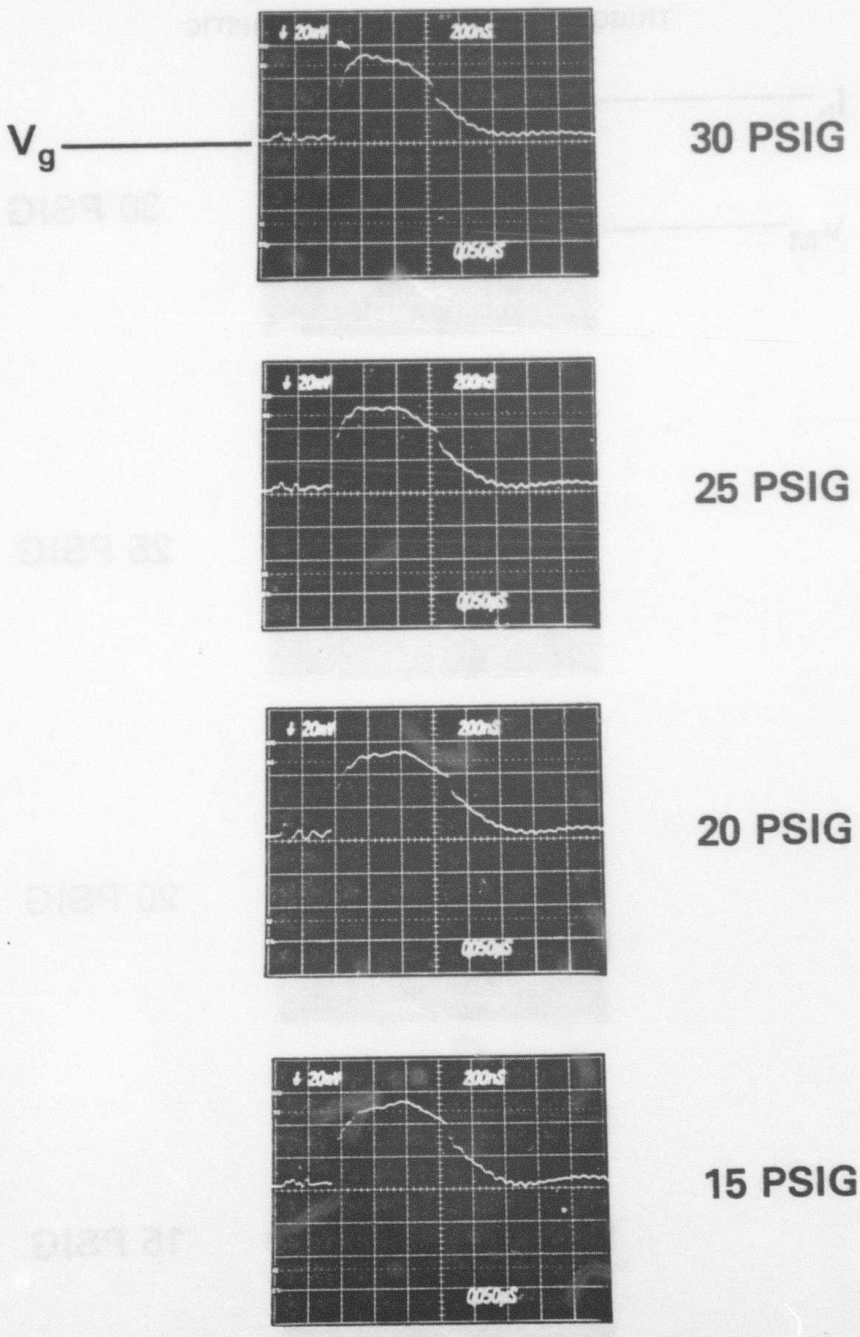

Fig. 3 - The voltage pulse incident to the foil as a function of peaking switch pressure is shown

TRIGGER RISE TIME CHARACTERISTIC

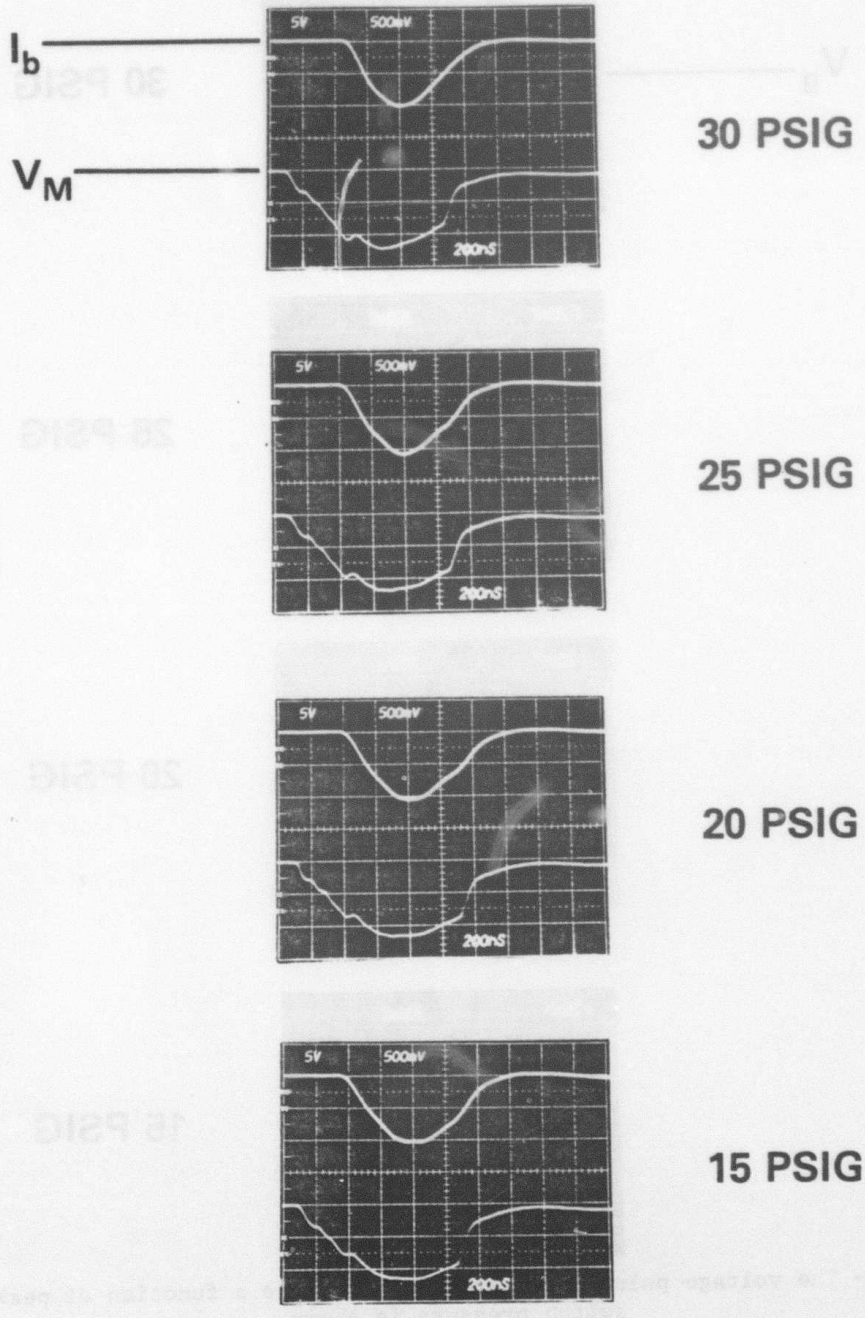

Fig. 4 - The current pulse incident to the foil as a function of peaking switch pressure is shown. The Marx voltage is also shown.

XeCl LASER COMPUTER MODELING

The XeCl laser modeling effort during the past fiscal year was mainly involved in the investigation of the long pulse e-beam pumped system. Some additional modeling was performed in support of an x-ray preionized, discharge pumped XeCl laser experiment. The modeling was done mainly in conjunction with experiments performed at NRL. For both systems, a large body of experimental and theoretical information regarding rate constants, electron-impact cross sections, photoabsorption cross sections, etc., had to be perused to develop realistic models. Most of the analysis for systems used computer codes previously developed at NRL over the past few years for modeling KrF, XeF, HgBr, and early XeCl lasers. Some additional code development was done to model the pulse forming line used in the x-ray preionized discharge pumped system. The discharge modeling is not discussed here except where its work overlaps the long pulse e-beam model.

A great deal of investigation of the literature was carried out to compile a good set of relevant reactions, rate constants, cross sections, etc. for modeling the e-beam pumped XeCl laser. Additional experiments were performed at NRL to determine, e.g., quenching rate constants. The rate constants used in the present model are listed in Table I. Some of the more important issues uncovered in the modeling and analysis are discussed below.

Stimulated emission cross section:

This is estimated from line width, $\Delta\lambda$, of the spontaneous emission, assuming homogeneous broadening, by

$$\sigma_{SE} = \lambda^4 \, (8\pi \, C \, \tau \, \Delta\lambda)^{-1}$$

where λ is the wavelength, τ is the spontaneous lifetime, C is the velocity of light and σ_{SE} is the stimulated emission cross section. Estimates of line width (FWHM) can be made from spontaneous spectra[1]. If one assumes a value of $\Delta\lambda$ = 25 Angstroms, and a spontaneous lifetime of 11 ns, then one derives $\sigma_{SE} = 4.34 \times 10^{-16}$ cm^2. A value consistent with this can be inferred from measurements[2] of saturation intensity, I_{sat}, and measurements[3] of quenching rate constants using

$$\sigma_{SE} = (\tau^{-1} + Q) \; / \; I_{sat},$$

from which is derived $\sigma_{SE} = 3.4 \times 10^{-16}$ cm^2 since, for the gas mixture used in reference 2, $\tau \; Q^{-1}$ 11 ns and I_{sat} = 0.35 MW cm^{-2}. Q is the total quenching rate for XeCl. This value of σ_{SE} is also consistent with a higher saturation intensity of $\sim$ 1 MW cm^{-2} observed in a discharge-pumped laser[4] where the gas mixture is such that the quenching exceeds the spontaneous rate by about a factor of 3.

HCl attachment and vibrational excitation:

Dissociative electron attachment to HCl in the ground vibrational state is asymptotically endoergic by more than half an eV. The published cross sections[5] for this state differ by about a factor of five but nonetheless are so low that the positive ion-negative ion recombination channel was originally assumed to contribute negligibly to the formation of the upper laser level, XeCl*. Recent experiments[6], however, have confirmed that the dissociative

electron attachment cross section of HCl increases dramatically with vibrational excitation. Indeed, for v=2, the attachment cross section was estimated to be 880 (± 50%) times larger than the cross section for v=0 near threshold. Since the production of Cl^- is an important factor in creating the upper laser level and in controlling the electron and ion balance, a reliable model of the XeCl laser (either discharge pumped or e-beam pumped) cannot be constructed unless a detailed knowledge of electron-impact vibrational excitation and dissociation and electron dissociative attachment of HCl is available. High quality absolute cross sections are much needed for this molecule for vibrational levels up to at least v=6. The rate constants listed in Table I represent effective rate constants which result in reasonable agreement with experiment over range of parameters which give good laser performance. It is by no means implied that these listed rate constants are the actual values.

Lower laser level removal:

Measured[7] rate constants for removal of the lower laser level of XeCl (X state) imply that a significant bottlenecking should occur at flux levels where most XeCl lasers operate. Even if one uses a multilevel model[8] of the XeCl (X) ground state, the observed extraction efficiency cannot be explained with the rates measured in reference 7. Various attempts to fit laser performance data with models over the past year have indicated that the XeCl (X) lifetime must be of the order of 0.5 ns or less in typical laser gas mixtures. A lifetime this short is reasonable if one recalls that the XeCl(X) is bound by only 255 cm^{-1}. Thus, it can be expected that almost every collision with a diluent gas molecule could result in dissociation (or, at least, removal from the v=1 and v=2 lower vibrational levels of the laser lines). This type of gas kinetic rate, at multiatmosphere pressures, can

result in a lower level lifetime in the subnanosecond range. Other possibilities which explain rapid lower laser level removal are electron collisions and, perhaps, spontaneous dissociation from rotational levels which lie above the dissociation limit of this extremely shallow potential well.

Electron quenching of XeCl*:

Early XeCl kinetics experiments[3] estimated that electron quenching in the e-beam pumped XeCl laser is not significant at e-beam current densities of up to 7 A cm^{-2}. This estimate gives evidence that the electron quenching rate for XeCl* is not as fast as that observed for other rare-gas halides[9]. A quenching rate constant of 2×10^{-8} cm^3 s^{-1} was inferred from modeling[10] high e-beam pump power experiments for pump powers up to 4000 kW cm^{-3}. This number is consistent with the 7 A cm^{-2} observations and indicates that the contribution of electron quenching to the total XeCl* quenching is in the range of a few percent.

Laser light absorption

The modeling done over the past year has indicated that the primary transient absorbing species for 308 nm radiation in an XeCl laser gas-mixture are Xe_2^+ and Cl^-. The photoabsorption cross section at 308 nm for Xe_2^+ has been calculated by Wadt[11] to be 2.4×10^{-17} cm^2 at 300 °K and is relatively insensitive to temperature at this wavelength. It should also be noted that species such as Xe_2^*, Se_2Cl^*, and Xe_3^+, because of their structural similarity to Xe_2^+, may have comparable photoabsorption cross sections. If one is to predict reliably the number densitites of these absorbers, one must have a good handle on all the reactions affecting these species. For example, the concentration of Xe_2^* is strongly dependent upon electron-impact processes creating and depleting the excited xenon levels, the recombination reactions which form Xe_2^* from the Xe* levels, and the radiative and collisional loss

rates of the various levels of Xe_2^*. Most of these rates are subject to varying degrees of uncertainty.

The electron photodetachment cross section for Cl^- at 308 nm has been measured[12] to be 1.1×10^{-17} cm^2. The exact effect of this large cross section on the total laser light absorption can only be calculated if one has a complete knowledge of all processes affecting the number density of Cl^-. As has been mentioned above, electron-impact processes such as vibrational excitation, dissociation, and attachment to HCl are not very well studied and much work needs to be done on these if one is to calculate accurately absorption by Cl^- in the XeCl laser.

Comparison of model with experiment

The rate constants and reactions listed in Table I have been incorporated into a computer code to model the long pulse e-beam pumped XeCl laser. This model predicts results in good qualitative agreement with observations of laser performance.

Some model predictions for a non-optimum XeCl laser mixture are compared with laser performance measurements in Figure 1. The ordinate is the average laser power efficiency which is defined as the ratio of the average laser output power emitted during a given time interval to the average electron beam energy per unit time deposited in the active laser volume during that time interval. This latter quantity is termed here the average power deposited and is the abscissa in Figure 1. The gas mixture for the data plotted in this figure was 2998 Torr neon, 40 Torr xenon, and 2.6 Torr HCl. The pump pulse was a slowly (approximately linear) rising e-beam with a peak current density incident to the active volume of 13.2 A/cm^2 and a total duration of 1 μs. The reflectivity product of the laser mirrors was 0.28 and the cavity length and gain length were 175 cm and 100 cm, respectively.

The point at 80 Joules per liter per microsecond in the Figure 1 corresponds to the total laser output efficiency over the whole pump pulse. The almost exact agreement between the observed and predicted efficiencies at this point is the result of "normalization" achieved by treating the effective stimulated emission cross section as an adjustable parameter and varying this quantity until the predicted specific laser output energy agreed with the observed (3.6 J/ℓ). The effective single-line stimulated emission cross section needed to obtain agreement was 1.2 $\mathring{A}^2$.

References

1. J. Tellinghuisen and M. R. McKeever, Chem. Phys. Lett. 72, 94 (1980).
2. L. F. Champagne, Appl. Phys. Lett. 33, 523 (1978).
3. T. G. Finn, R. S. F. Chang, L. F. Palumbo, and L. F. Champagne, Appl. Phys. Lett. 36, 789 (1980).
4. B. L. Wexler and L. J. Palumbo, "Experimental and Theoretical Performance Characteristics of an X-ray Preionized, 100 ns Discharge XeCl Laser," 33rd Annual Gaseous Electronics Conference, Norman, OK (Oct. 1980).
5. R. Azria, L. Roussier, R. Paineau, and M. Tronc, Rev. Phys. Appl. (Paris) 9, 469 (1974); Also, L. G. Christophorou, R. N. Compton, and H. W. Dickson, J. Chem. Phys. 48, 1949 (1968).
6. M. Allan and S. F. Wong, J. Chem. Phys. 74, 1687 (1981).
7. R. W. Waynant and J. G. Eden, Appl. Phys. Lett. 36, 262 (1980).
8. S. F. Fulghum, M. S. Feld, and A. Javan, IEEE J. Quantum Electron, QE-16, 815 (1980).
9. D. W. Trainor, J. H. Jacob, and M. Rokni, J. Chem. Phys. 72, 3646 (1980).
10. W. L. Morgan and M. J. Pound, "Kinetics of E-Beam Excited XeCl," paper FB-3, 33rd Annual Gaseous Electronics Conference, Norman, OK (Oct. 1980).
11. W. R. Wadt, J. Chem. Phys. 73, 3915 (1980).

References for Table I

R1. C. H. Fisher, R. E. Center, and J. P. McDaniel, "Radiative Lifetime and Collisional Quenching Kinetics for the XeCl (B 1/2) State," Paper AB-3, 32nd Annual Gaseous Electronics Conf., Pittsburgh, PA (Oct. 1980).

R2. See text.

R3. T. G. Finn, R. S. F. Chang, L. J. Palumbo, and L. F. Champagne, Appl. Phys. Lett. 36, 789 (1980).

R4. W. L. Morgan and M. J. Pound, Paper FB-3, 33rd Annual Gaseous Electronics Conf., Norman, OK (Oct. 1980).

R5. W. R. Wadt, J. Chem. Phys. 73, 3915 (1980).

R6. K. J. McCann and M. R. Flannery, Appl. Phys. Lett. 31, 599 (1977).

R7. J. M. Hoffman and J. B. Moreno, "Three Body Ion-Ion Recombination Coefficients for Rare-Gas-Halogen Mixtures," Sandia National Lab. Report SAND80-1486, (Aug. 1980).

R8. J. H. Kolts, J. E. Velazco, and D. W. Setser, J. Chem. Phys. 71 (1979).

R9. R. S. F. Chang, experiments performed at NRL (See elsewhere in this report).

R10. R. Johnsen, A. Chen, and M. A. Biondi, J. Chem. Phys. 73, 1717 (1980); Also, J. D. C. Jones, D. G. Lister, D. P. Wareing, and N. D. Twiddy, J. Phys. B: Atom. Molec. Phys. 13, 3247 (1980).

R11. H. Helm, Phys. A 14, 680 (1976).

R12. C. B. Collins and F. W. Lee, J. Chem. Phys. 72, 5381 (1980).

R13. J. M. Brom, Jr., J. H. Kolts, and D. W. Setser, Chem. Phys. Lett. 55, 44 (1978).

R14. R. H. Neynaber and S. Y. Yang, to be published in Phys. Rev. A. (Early 1981).

R15. L. Frommhold, M. A. Biondi, and F. J. Mehr, Phys. Rev. 165, 44 (1968); Also, J. Philbrick, F. J. Mehr, and M. A. Biondi, Phys. Rev. 181, 271 (1969).

Notes for Table I:

N1. XeCl* represents the lumped (closely coupled) B and C states. The lasing transition is assumed to be lumped into a single line.

N2. XeCl represents the XeCl(X) vibrational levels which can absorb laser radiation. Any other XeCl(X) vibrational levels are lumped with Xe + Cl and hence do not contribute to resonant reabsorption of laser light.

N3. P_f represents a fluorescence photon at the laser wavelength.

N4. P_i represents an axial intracavity laser photon.

N5. The "solid angle factor," Ω, is an estimate of the fraction of the spontaneous radiation emitted in a sufficiently small angle to the laser axis to be subject to amplification and absorption. Predictions of laser performance are relatively insensitive to the exact value chosen for this factor.

N6. P_o represents a laser photon which is transmitted by the output coupler 1 laser light output.

N7. This formulation assumes a "uniform gain" approximation in which 1_c is the cavity length, c is the velocity of light, and R_1R_2 is the reflectivity product for the cavity mirrors.

N8. This value of σ_{SE} is approximately equivalent to assuming that half the population of XeCl* is in the C-state reservoir and that the actual value of σ_{SE} is twice that given.

N9. Required to be consistent with experiments (see text).

N10. Assumed to be the same photoabsorption cross section for Xe_2^+ because of similar molecular structure.

N11. Most likely products.

N12. Analogy with Xe_2^+.

N13. Effective two-body rate coefficient for diluent (Ne) pressure of 4 amagats. These rates vary somewhat with diluent gas and concentration (see reference R7).

N14. 100% branching into XeCl* is assumed.

N15. Assumed by analogy from above reactions.

N16. Branching ratio to form XeCl* is stated by the authors of reference R8 to be less than 2%. The reaction is slightly endoergic.

N17. For the purpose of the present model, and since the reaction is exoergic the branching ratio into XeCl* is assumed to be unity. The contribution of these neutral channels to the total XeCl* formation is about 5-10%.

N18. Rate constant guessed by analogy to rate for Xe*(6s) + HCl(v=0) reaction.

N19. Guessed from analogous rate constants in listed in reference R10.

N20. Based on assumed forward rate and the equilibrium constant measured in reference R11.

N21. This rapid three-body rate beats the electron dissociative recombination followed by Penning ionization route by at least a factor of five in contributing to the formation of Xe^+.

N22. Branching of 75% Penning ionization and 25% associative ionization is assumed analogous to other systems.

N23. Rate derived from published cross sections near room-temperature energies.

N24. The rate constant is given for an electron temperature of 1 eV.

N25. Analogy from above reaction.

N26. Analogy with NeF* rapid predissociation.

N27. Ionization and excitation by the electron beam are computed using the secondary electron kinetics treatment discussed in the NRL-DARPA report for FY 79. Typical proportioning of the incident fast-electron energy for gas mixtures modeled here is approximately 59% into creating Ne^+, 13% into Ne*, 8% into Xe* and Xe^+, and 20% into translational energy of the diluent.

N28. The listed rate constants are effective values which produce reasonable agreement with experiment. Usually, they are computed using cross sections and the electron energy distribution function computed from the secondary electron kinetics code.

TABLE I: REACTIONS AND RATE CONSTANTS USED IN THE PRESENT XeCl LASER MODEL

Lasing and fluorescence	Rate Constant or Rate	Reference	Notes
$XeCl^* \rightarrow XeCl + P_f$	$\tau = 16$ ns	R1	N1, N2, N3
$XeCl^* \rightarrow XeCl + P_i$	$\Omega \approx 10^{-7}$	R1	N4, N5
$P_i \rightarrow P_o$	$\tau_c^{-1} = -(C/2\ell_c)\ \ell n\ (R_1R_2)$	R1	N6, N7
$XeCl^* + P_i \rightarrow XeCl + 2\ P_i$	$\sigma_{SE} = 1.4\ \mathring{A}^2$	R2	N8
$XeCl + P_i \rightarrow XeCl^*$	$\sigma_{SE} = 1.4\ \mathring{A}^2$		
$XeCl + M \rightarrow Xe + Cl + M$	$\tau < 0.5$ ns		N9
Quenching			
$XeCl^* + Ne \rightarrow Xe + Cl + Ne$	1.0 (-12)	R3	
$XeCl^* + Xe \rightarrow Xe + Cl + Xe$	3.2 (-11)	R3	
$XeCl^* + 2\,Ne \rightarrow Xe + Cl + 2\,Ne$	< 1.0 (-33)	R3	
$XeCl^* + HCl \rightarrow Xe + Cl + HCl$	1.4 (-9)	R3	
$XeCl^* + e^- \rightarrow Xe + Cl + e^-$	2.0 (-8)	R4	

TABLE I: (Continued) REACTIONS AND RATE CONSTANTS USED IN THE PRESENT XeCl LASER MODEL

Absorption of Laser Photons	Rate Constant or Rate	Reference	Notes
$Xe_2^+ + P_i \rightarrow Xe^+ + Xe$	$\sigma = 0.24\ \mathring{A}^2$	R5	
$Xe_3^+ + P_i \rightarrow Xe^+ + 2\ Xe$	$\sigma \approx 0.24\ \mathring{A}^2$		N10, N11
$Xe_2Cl^* + P_i \rightarrow Xe^+ + e^- + Xe + Cl$	$\sigma \approx 0.24\ \mathring{A}^2$		N10, N11
$Xe_2^* + P_i \rightarrow Xe^+ + e^- + Xe$	$\sigma \approx 0.24\ \mathring{A}^2$		N10, N11
$Ne_2^+ + P_i \rightarrow Ne^+ + Ne$	$\sigma = 0.01\ \mathring{A}^2$	R5	
$Ne\ Xe^+ + P_i \rightarrow Xe^+ + Ne$	$\sigma = 0.02\ \mathring{A}^2$		N11, N12
$Xe^* + P_i \rightarrow Xe^+ + e^-$	$\sigma = 0.0006\ \mathring{A}^2$	R6	
$Ne^* + P_i \rightarrow Ne^+ + e^-$	$\sigma < 0.0001\ \mathring{A}^2$	R6	

TABLE I: (Continued) REACTIONS AND RATE CONSTANTS USED IN THE PRESENT XeCl LASER MODEL

Ion Formation Channel	Rate Constant or Rate	Reference	Notes
$Xe^+ + Cl^- \rightarrow XeCl^*$	2.0 (-6)	R7	N13
$Xe_2^+ + Cl^- \rightarrow XeCl^* + Xe$	1.9 (-6)	R7	N13, N14
$Ne\ Xe^+ + Cl^- \rightarrow XeCl^* + Ne$	2.0 (-6)	R7	N13, N14
$Xe_3^+ + Cl^- \rightarrow XeCl^* + 2\ Xe$	2.0 (-6)		N15
Neutral Formation Channel			
$Xe^*(6s) + HCl\ (v=0) \rightarrow$ Products	5.6 (-10)	R8	N16
$Xe^*(6s) + HCl\ (v>0) \rightarrow XeCl^* + H$	>2.0 (-10)	R9	N17
$Xe^*(6s') + HCl \rightarrow XeCl^* + H$	5.0 (-10)		N17, N18
$Xe^{**} + HCl \rightarrow XeCl^* + H$	5.0 (-10)		N11, N18

TABLE I: (Continued) REACTIONS AND RATE CONSTANTS USED IN THE PRESENT XeCl LASER MODEL

Xenon Ion Cascade	Rate Constant or Rate	Reference	Notes
$Xe^+ + Xe + M \rightarrow Xe_2^+ + M$	1.0 (-31)	R10	N19
$Xe^+ + 2\,Ne \rightarrow Ne\,Xe + Ne$	1.0 (-31)		N19
$Ne\,Xe^+ + Ne \rightarrow Xe^+ + 2\,Ne$	2.8 (-13)		N20
$Xe_2^+ + Xe + M \rightarrow Xe_3^+ + M$	1.0 (-31)		N19
$Xe_3^+ + M \rightarrow Xe_2^+ + Xe + M$	2.8 (-13)	R11	N20
Formation of Xe^+			
$Ne_2^+ + Xe + M \rightarrow Xe^+ + 2\,Ne + M$	3.9 (-30)	R12	N21
$Ne_2^+ + Xe \rightarrow Xe^+ + 2\,Ne$	< 5.0 (-11)	R12	
$Ne^* + Xe \rightarrow Xe^+ + Ne + e^-$	5.6 (-11)	R13	N22
$Ne^* + Xe \rightarrow Ne\,Xe^+ + e^-$	1.9 (-11)	R13	N22
$HCl^+ + Xe \rightarrow Xe^+ + HCl$	3.4 (-10)	R14	N23

TABLE I: (Continued) REACTIONS AND RATE CONSTANTS USED IN THE PRESENT XeCl LASER MODEL

Neon Ion Kinetics	Rate Constant or Rate	Reference	Notes
$Ne^+ + 2\,Ne \rightarrow Ne_2^+ + Ne$	6.4 (-32)	R10	
$Ne_2^+ + e^- \rightarrow Ne^* + Ne$	3.5 (-8)	R15	N24
$Ne^+ + Cl^- \rightarrow (NeCl^*)$	3.2 (-6)	R7	N13
$Ne_2^+ + Cl^- \rightarrow (NeCl^*)$	3.2 (-6)		N13, N25
$(NeCl^*) \rightarrow Cl^+ + e^- + Ne$	τ = 0.5 ns		N11, N26
Pumping			
$Ne, Xe + e^{-beam} \rightarrow Ne^+, Ne^*, Xe^+, Xe^*$			N27
Attachment and vibrational excitation			
$HCl\ (v=0) + e^- \rightarrow Cl^- + H$	1.0 (-10)	R2	N28
$HCl\ (v>0) + e^- \rightarrow Cl^- + H$	1.0 (-8)	R2	N28
$HCL\ (v=0) + e^- \rightarrow HCl\ (v>0) + e^-$	3.0 (-8)	R2	N28
$HCL\ (v>0) + e^- \rightarrow HCl\ (v=0) + e^-$	3.0 (-8)	R2	N28

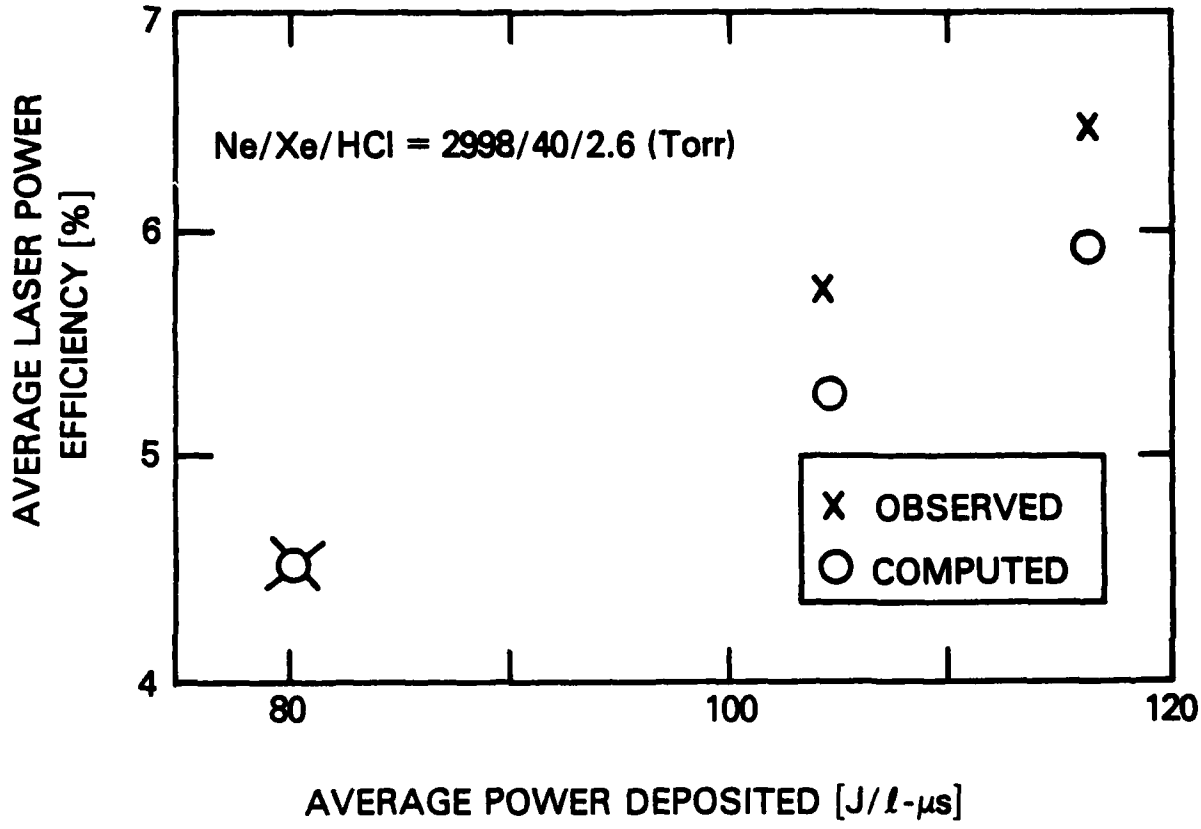

Fig. 1 - XeCl laser power efficiency versus e-beam pump rate

GROUND STATE DESTRUCTION OF XeF AND XeCl

Rare gas halide excimer laser development has shown great favoritism to two molecules, XeF and XeCl, which have bound lower levels. In the case of XeF,[1-3] the potential well is about 1155 cm^{-1} and the well contains about 10 vibrational levels. For XeCl[4] the potential well is only ~ 250 cm^{-1} (~ KT at room temperature) and the well contains about 12 vibrational levels. For laser calculations it is important to know how rapidly population is removed from the lower laser levels since a population buildup in the lower laser level will destroy the population inversion and terminate lasing.

In spite of the importance of lower state removal, few studies of the process have been conducted. For XeF, studies have been done by Fulghum, Feld and Javan at MIT.[5-7] These researchers have investigated the time dependence of the XeF ground state vibrational levels v"=0 and v"=1 using two different experimental approaches. Their first method[5] used a dye laser to probe a F_2:Xe:He gas mixture excited by a short discharge. Ground state information was obtained by probing the XeF(X→B) absorption on selected transitions in the afterglow of the discharge. A rate constant of 1×10^4 sec^{-1} $Torr^{-1}$ for destruction of v"=0 by He was measured. Their second method[6] produced XeF by photolysis of XeF_2. They then observed the B→X emission which followed XeF(X→B) absorption of a dye laser pulse which was tuned to a selected X→B transition. This method allowed more selectivity in the observations and yielded a destruction rate constant of 1.4×10^4 sec^{-1} $Torr^{-1}$ for v"=0 for He. The same value was obtained for v"=1. Since the rate constants for v"=0 and v"=1 were the same, Fulghum et al. concluded that rapid equilibration must take place among the vibrational levels and that this equilibration lowers the effective lifetimes of each level to a value sufficiently short to account for the absence of bottlenecking in laser experiments. These authors have constructed a multilevel model[7] which yielded results supporting their conclusion. They also observed the same rate constant for Ne and have concluded that all molecules had about the same destruction rate constant.

Experiments with XeCl have been conducted previously by Waynant and Eden[8] at NRL with DARPA support and extensions of this work are reported here. These experiments were done using an electron-beam-excited mixture of Ne:Xe:HCl probed by a tunable dye laser. Destruction rates were obtained by monitoring XeCl(X→B) absorption of the dye laser probe when two constituents were held at constant pressure and the third varied in pressure. Destruction rate constants were obtained for HCl, Xe, Ne and Ar for v"=0 and for v"=1 and 2 for Ne. A copy of the published results of this work is attached. The rate constants measured for Ne were the same for v"=0, 1 and 2 leading to the conclusion that rapid equilibration occurs in ground state XeCl also. The destruction rates for HCl and Xe were much faster than the destruction rate of Ne. This followed the trend observed in quenching of the B state where halogen donors were the most active quenchers and Xe was the most active quencher of the rare gas atoms.

In a rather similar experiment Hutchinson et al.[9] probed an electron beam excited HCl:Xe:Ne mixture with a picosecond pulse train tuned to XeCl(X→B) transitions. Analysis of the population in v"=0 and 1 showed a binary exponential decay. The first part showed a decay time of about 20 ns and the second part a decay of about 250 ns. The break in the curve occurs at about 40 ns or approximately where the e-beam turned off. Hutchinson attributed the 20 ns decay to the actual destruction of ground state vibrational levels and the 250 ns decay to an equilibrium ground state XeCl concentration due to "chemical scavenging of free Cl." According to Strong[10] it is the long lifetime of Cl that accounts for his ability to measure XeCl ground state absorption[11] 80 μsec after flash photolyzing Cl_2 in Xe/Cl_2 mixtures. Similar observations for XeF have been made by Smith and Kobrinsky.[12]

The absolute values of the XeCl destruction rate constants measured by Waynant and Eden has caused difficulty since these values lead to ground state lifetimes much too long to account for experimental laser observations. Even if the rapid equilibration postulated were to reduce the lifetime by a factor of 10-12, the numerical model would not agree with experiment. Indeed, a further reduction of a factor of 50 ($\tau \approx 0.1$-0.3 ns) is needed for agreement between model and experiment.

In an effort to resolve the questions regarding the ground state behavior, experiments have been conducted with both XeF and XeCl. Because photolysis of

XeF_2 forms excited state XeF(B, etc.) without a combination of gases and a combination formation chain, it was chosen as the method for investigating the ground state of XeF. The basis of the experiment required the synchronization of a Febetron 706 e-beam and a tunable dye laser. The Febetron excited a Ar/Cl_2 mixture producing 175 nm radiation which photolyzed the XeF_2 in a quartz cell. This produced XeF(B, etc.) which rapidly decayed into the ground vibrational levels according to the Franck-Condon factors. When the dye laser was tuned to X→B transitions, the population was proportional to the dye laser absorption. In these experiments the dye laser was carefully set to the XeF(B, v'=0←X, v"=2) transition at 351.1 nm by superimposing the dye laser and a Ne calibration spectrum on a PAR OMA display following dispersion with a 0.5 m Minuteman spectrograph. When about 1 Torr XeF_2 and 10 Torr He were admitted to the cell, the lifetime of the absorption lasted longer than the width of the probe pulse. By changing the timing between the Febetron and dye laser and then integrating under the probe beam signal, it was possible to crudely plot the relative absorption as a function of time, i.e., the relative ground state population in v"=2 as a function of time. This curve is shown in Fig. 1. The decay time is about 2.6 μsec which is in reasonable agreement with the values obtained by Fulghum for v"=0 and v"=1 for He. These results further support the contention that the vibrational levels rapidly equilibrate. It is difficult, however, to support the contention that all molecules destroy XeF with a similar rate constant. If one compares the destruction rates measured in Fulghum's two experiments, one experiment a gas mixture of 1.2 Torr F_2, 6 Torr Xe and 10 Torr He[5] and the other experiment containing only XeF and 10 Torr He, two data points are obtained which would yield a rate constant of 1.6×10^{-11} $cm^3 \cdot sec^{-1}$ for F_2 destruction. This assumes in the gas mixture that 1.2 Torr F_2 is the dominant destroyer compared to 6 Torr Xe which quenching experiments always holds true. Interestingly, the destruction rate for XeF(X) by F_2 is in close agreement with the value obtained by Eden and Waynant for XeCl(X) destruction by HCl in the earlier XeCl ground state studies. It should be possible to directly measure the destruction rate constants for F_2, Xe, etc. in the XeF photolysis experiment and this is in progress.

Further experiments to investigate the ground state behavior of XeCl utilized apparatus similar to the photolysis experiment except that the electron beam was used to directly excite a gas mixture of HCl:Xe:Ne

(1 Torr:10 Torr:400 Torr). This same approach had previously yielded considerable absorption and decay times of hundreds of nanoseconds. All attempts to repeat the previous results have failed. The results of the present experiments all indicated that any absorption (i.e., any population) associated with the 308.2 (0-2), 305.8 (1-0), 304.3 (2-1) or the 309.1 (0-6) transition decayed in $\lesssim$ 1 ns. As yet no effects due to gas purity, linewidth of the probe, or exact wavelength setting can be found to explain the different results. The present feeling is that the most likely cause of the discrepancy is that ground state XeCl was being generated by long lived Cl in the earlier experiment. This would have slowed the destruction rate and would have led to long lifetimes similar to those seen by Hutchinson after his e-beam turned off. Further investigations of this are in progress.

References

1. J. Tellinghuisen, G. C. Tisone, J. M. Hoffman and A. K. Hays, J. Chem. Phys. 64, 4796 (1976).
2. J. Tellinghuisen, P. C. Tellinghuisen, G. C. Tisone, J. M. Hoffman and A. K. Hays, J. Chem. Phys. 68, 5187 (1978).
3. P. C. Tellinghuisen, J. Tellinghuisen, J. A. Coxon, J. E. Velazco and D. W. Setser, J. Chem. Phys. 68, 5177 (1978).
4. J. Tellinghuisen, J. M. Hoffman, G. C. Tisone and A. K. Hays, J. Chem. Phys. 64, 2484 (1976).
5. S. F. Fulghum, I. P. Herman, M. S. Feld and A. Javan, Appl. Phys. Lett. 33, 926 (1978).
6. S. F. Fulghum, M. S. Feld and A. Javan, Appl. Phys. Lett. 35, 247 (1979).
7. S. F. Fulghum, M. S. Feld and A. Javan, IEEE JQE, QE-16, 815 (1980).
8. R. W. Waynant and J. G. Eden, Appl. Phys. Lett. 36, 262 (1980).
9. M. H. R. Hutchinson, C. D. P. Levy and G. M. Reksten, "Vibrational Relaxation Studies in Noble Gas Halides" in Laser Advances and Applications, John Wiley, New York, 1980, pp. 57-60.
10. R. L. Strong, private communication.
11. S. L. Shostak and R. L. Strong, Chem. Phys. Lett. 63, 370 (1979).
12. A. L. Smith and P. C. Kobrinsky, J. Mol. Spectrosc. 69, 1 (1978).

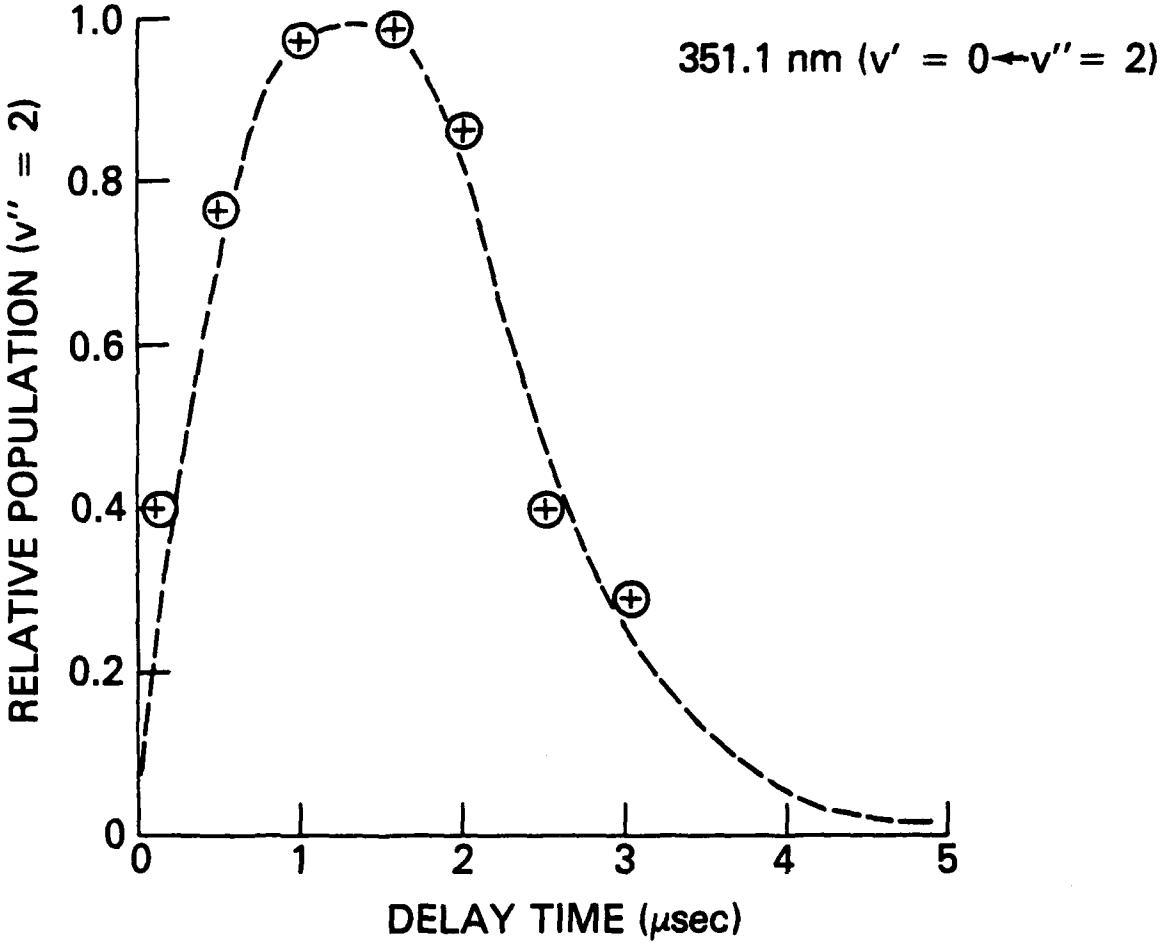

Fig. 1 - Relative population of XeF(X, v''=2) with 10 Torr He as a function of time

Destruction of ground state XeCl molecules by HCl and rare gas collisions

R. W. Waynant and J. G. Eden[a)]
Naval Research Laboratory, Washington, D.C. 20375

(Received 19 October 1979; accepted for publication 4 December 1979)

Rate constants for quenching of several XeCl (X) vibrational levels by the rare gases and HCl have been measured. The temporally resolved decay of the population densities of the XeCl (X, $v'' = 0$–2) levels was monitored using a frequency-doubled tunable dye laser. Within experimental error, the measured rate constants did not vary with vibrational number, and the temperature dependence of the rates over the range $300 < T < 375$ °K was found to be consistent with the previously measured XeCl (X) dissociation energy (~ 250 cm^{-1}). The rate constants for the destruction of XeCl (X, $v'' = 0$) state molecules by HCl, Xe, Ar and Ne at 300 °K were determined to be $(2.2 \pm 0.5) \times 10^{-11}$, $(5.6 \pm 0.8) \times 10^{-12}$, $(0.6 \pm 0.06) \times 10^{-13}$, and $(1.0 \pm 0.15) \times 10^{-13}$ cm^3 sec^{-1}, respectively.

PACS numbers: 82.20.Pm, 42.55.Hq, 82.40.Tc, 34.90. + q

Several important rare-gas halide molecules, XeF, XeCl, and perhaps XeBr,[1] have bound ground states. Consequently, the collisional destruction and dissociation rates for the ground-state vibrational levels of these molecules are significant factors in determining laser performance. Fulghum and coworkers previously have studied[2,3] the collisional decay rates for low-lying vibrational levels of the XeF (X) state and have concluded[3] that VT processes rapidly equilibrate the X state vibrational manifold, and that the various vibrational levels decay at a common rate with dissociation primarily occurring from the highest v'' levels.

From an analysis of the XeCl emission spectrum, Tellinghuisen *et al.* determined[4] the XeCl (X) dissociation energy to be ~ 255 cm^{-1}. Their studies indicated that 12 vibrational levels lie within the X state potential well. Further verification of the bound nature of the XeCl (X) state has been provided by Shostak and Strong[1] who, in recent photolysis experiments, observed transient uv absorption spectra corresponding to the XeCl $X \rightarrow B$ ($\lambda_{max} \sim 308$ nm) and $X \rightarrow D$ (236 nm) bands.

Rate constants for collisional quenching of the XeCl (X, $v'' = 0$–2) levels by HCl and the rare gases have been measured and are reported here. These rates were determined by monitoring the exponential time decay of the population of the desired ground-state vibrational level in the presence of a background gas mixture. In agreement with the results of Fulghum,[3] the rate constants measured in this work, within experimental error, were not found to depend on vibrational number. Also, the temperature dependence of the decay rates was examined and found to be consistent with $200 < D_0$ [XeCl (X)] < 300 cm^{-1}.

Figure 1 is a simplified energy level diagram for XeCl indicating the vibrational transitions studied. Temporal resolution of the density of a particular v'' level was obtained by observing the absorption of dye laser radiation on the (1–0), (0–2), and (2–1) transitions of the XeCl ($B \rightarrow X$) band. The wavelengths for these transitions are 305.9, 308.2, and 304.4 nm, respectively.

The experimental apparatus used for these studies is shown schematically in Fig. 2. A frequency-doubled dye laser, which could be tuned from 280 to ~ 320 nm, was used as the optical pump. The output of the laser had a pulse duration of ~ 1 μs FWHM. The pulse contained approximately 1 mJ of energy and had a spectral linewidth of ~ 0.1 nm. After the beam was filtered to eliminate the fundamental frequency, it was split into two beams, one of which was passed through a stainless steel cell mounted on a Febetron 706 electron beam generator. From the vibrational level assignments of Tellinghuisen,[4] the dye laser wavelength was set to the desired vibronic transition of the $X \rightarrow B$ band using a 0.5-m Minuteman monochromator. Both the laser pulse transmitted through the gas cell and the reference signal were detected by photomultipliers and displayed on a dual-beam oscilloscope. To equalize their amplitude response and to suppress fluorescence from the e-beam cell, calibrated

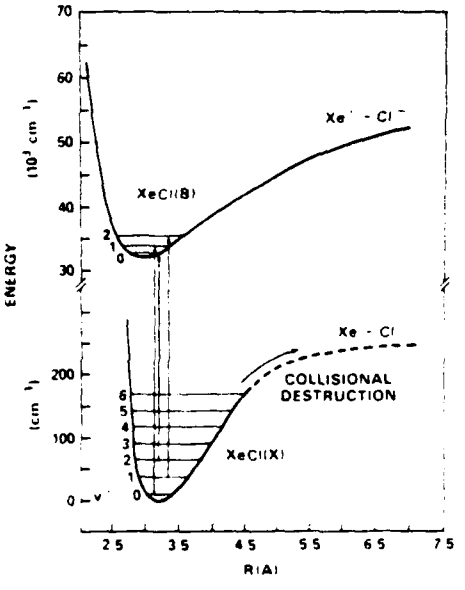

FIG. 1. Partial energy level diagram for the XeCl molecule showing the absorption transitions probed by the dye laser to study the populations in $v'' = 0$, 1, and 2 levels of the X state.

a)Present address: Department of Electrical Engineering, University of Illinois, Urbana, IL 61801

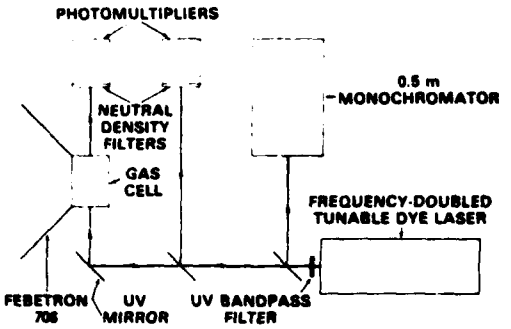

FIG. 2. Schematic diagram of the experimental apparatus. The gas cell contained Ne/Xe/HCl gas mixtures typical of those used in e-beam pumped XeCl lasers.

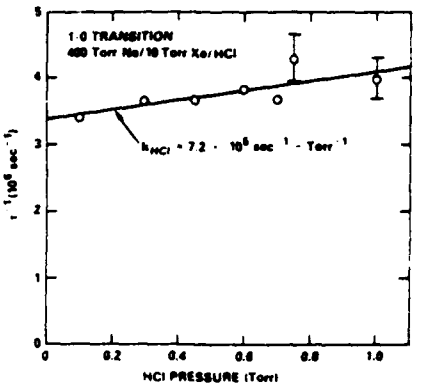

FIG. 4. Dependence of the exponential absorption decay constant (τ^{-1}) on the partial pressure of HCl in Ne/Xe/HCl gas mixtures. The graph reflects the decay of the $v'' = 0$ level of the X ground state and the two error bars shown are representative of the uncertainty (standard deviation = $\pm 1.7 \times 10^5$ sec^{-1} Torr^{-1}) in the data.

quartz neutral density filters were placed in front of the photomultipliers.

Data were taken with Ne/Xe/HCl (400 : 10 : 1) gas mixtures in the gas cell that are typical of those used in e-beam pumped XeCl lasers. The use of Cl_2 for these experiments was undesirable due to its broadband absorption in the 300-nm spectral region. Research grade purity rare gases were used for these experiments and the HCl purity was better than 99% (technical grade). All of the gases were used without further purification.

Roughly 100 ns after the start of the dye laser pulse, an intense (~ 1 kA cm^{-2}) $\sim$ 3-ns FWHM electron beam from the Febetron 706 entered the gas cell, creating XeCl (B) state molecules. The subsequent radiative decay of the XeCl* molecules populated several vibrational levels of the ground state which, in turn, were eventually destroyed through collisions with the background gas.

An oscillogram illustrating absorption by the XeCl (X, $v'' = 0$) state in e-beam excited 98.6% Ne/1.2% Xe/0.2% HCl ($P_{TOTAL} \sim 800$ Torr) gas mixtures is shown in Fig. 3. Following the excitation of the gas mixture, spontaneous emission lasting ~ 100 ns was observed followed by strong absorption which persisted for ~ 300 ns. This absorption was observed *only* when both Xe and HCl were present in the Ne gas.

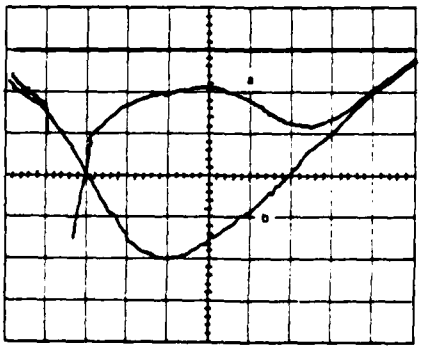

FIG. 3. Oscillogram of XeCl (X) absorption in e-beam excited 98.6% Ne/1.2% Xe/0.2% HCl ($P_{TOTAL} \sim 800$ Torr) gas mixture. The transition probed is the 1–0 line (305.9 nm) and both the transmitted (a) and incident (b) laser signals are shown. The initial surge in the signal transmitted by the gas cell is due to XeCl ($B \rightarrow X$) fluorescence. Scales are 100 ns/div and 10 mv/div.

Oscillograms similar to Fig. 3 were recorded for various Ne/Xe/HCl gas mixtures (varying one constituent of the mixture while keeping the other two constant) and for the three $X \rightarrow B$ vibronic transitions mentioned earlier. For all of the gas mixtures studied, the time dependence of the ground state absorption [$\sim \ln(I/I_0)$, where I and I_0 are the the transmitted and incident signal intensities, respectively] showed that the population of the X state vibrational level under study decayed exponentially over several time constants. Previous studies of the emission from Febetron excited Ne/Xe/HCl gas mixtures had shown that the XeCl ($B \rightarrow X$) fluroresence terminated 10–200 ns after the initiation of the e-beam pulse. Therefore, the extraction of exponential decay constants from the absorption data was performed 300–600 ns into the afterglow of the plasma.

Figure 4 shows the dependence of the exponential absorption decay constant (τ^{-1}) on the partial pressure of HCl. The 1–0 transition was probed by the dye laser and so the data reflect the decay of the XeCl (X, $v'' = 0$) state. The linear least-squares fit to the data is represented by the solid line. From the slope of this line, the rate constant for quenching of the $v'' = 0$ level by HCl was determined to be $(2.2 \pm 0.5) \times 10^{-11}$ cm^3 sec^{-1}. The uncertainty given represents the standard deviation of the data about the least-square linear fit. Table I summarizes the rate constants for quenching of several X state vibrational levels that were measured in these experiments. No dependence of the Ne quenching rate constants on the vibrational level (v'') probed was observed. This is in agreement with previous work on XeF.[3]

The rate constants presented here differ widely for the various quenching gases investigated. This represents a departure from the results of Fulghum and coworkers.[3] In their studies of collisional equilibration in the XeF ground

TABLE I. Summary of the rate constant for quenching of the X state $v'' = 0$–2 vibrational levels at $T = 300$ °K by HCl and the rare gases.

Transition Probed $v' - v''$ (λ, nm) [a]	Quencher	k_Q(cm^3 sec^{-1})
	HCl	$(2.2 \pm 0.5) \times 10^{-11}$
	Ne	$(1.0 \pm 0.15) \times 10^{-13}$
1–0 (305.9)		
	Ar	$(0.6 \pm 0.06) \times 10^{-13}$
	Xe	$(5.6 \pm 0.8) \times 10^{-12}$
2–1 (304.3)	Ne	$(1.0 \pm 0.13) \times 10^{-13}$
0–2 (308.2)	Ne	$(1.0 \pm 0.07) \times 10^{-13}$

[a] Reference 4.

state, the decay rates for the $v'' = 1$ level using He and Ne buffers were found to be the same to within experimental error. This discrepancy could be due to the rather similar collisional cross sections for He and Ne which would have hidden the differences in the XeF experiment. The larger rate constants observed here are for Xe and HCl which would have larger collisional cross sections. An alternative explanation could be that dissociation from all v'' levels is more important for XeCl, which has a low binding energy ($\sim kT$ or 255 cm^{-1}), than it is for the low-lying levels of XeF (X).

The temperature dependence of the rate constants in Table I was also investigated by heating the e-beam gas cell. Heating tape was wrapped around the cell and a chromel-alumel thermocouple was positioned inside the cell immediately adjacent to the path of the probe laser. With this arrangement, temperatures in the range 300 to 375 °K could be studied. As the cell temperature was elevated, the rate constants were found to obey the relationship $k_Q \sim \exp(-\Delta E/kT)$ where $200\ \text{cm}^{-1} < \Delta E = D_0(X) < 300\ \text{cm}^{-1}$, which is consistent with the ground-state dissociation energy reported by Tellinghuisen.[4] Also, for temperatures in excess of ~ 350 °K, the XeCl fluorescence and, hence, the ground-state absorption decreased dramatically, which could be due to reaction of HCl with the cell walls.

In summary, the rate constants for quenching of the $v'' = 0$–2 levels of the XeCl ground state by HCl and the rare gases have been measured. Within the experimental error, the rate constants did not depend on v'' and the temperature dependence of the rates over the range $T = 300$–375 °K was found to be consistent with the X state dissociation energy measured previously. Knowledge of the XeCl (X) quenching rate constants reported here are useful for modeling of quasi-steady-state (> 0.5-μs pulse length) XeCl lasers.

The authors gratefully acknowledge the partial financial support of DARPA, discussions with N. Djeu and C.H. Fisher, and the technical assistance of D. Epp and K. Tayman.

[1] S.L. Shostak and R.L. Strong, Chem. Phys. Lett. 63, 370 (1979).
[2] S.F. Fulghum, I.P. Herman, M.S. Feld, and A. Javan, Appl. Phys. Lett. 33, 926 (1978).
[3] S.F. Fulghum, M.S. Feld and A. Javan, Appl. Phys. Lett. 35, 247 (1979).
[4] J. Tellinghuisen, J.M. Hoffman, G.C. Tisone, and A.K. Hays, J. Chem. Phys. 64, 2484 (1976).

XeF(C) state lifetime and quenching by rare gases and fluorine donors

R. W. Waynant
Naval Research Laboratory, Washington, D.C. 20375

(Received 12 November 1979; accepted for publication 7 January 1980)

The lifetime and quenching rate constants for the XeF(C) state have been measured when that state is produced by flash photolysis of XeF_2 in the presence of such quenching gases as He, Ne, N_2, Xe, Ar, XeF_2, NF_3, and F_2. The lifetime measured in this manner is 95 ± 7 ns and the quenching rate constants are 1.2×10^{-13}, 3×10^{-13}, 4×10^{-13}, 1×10^{-12}, 9×10^{-14}, 1.7×10^{-10}, 1.6×10^{-11}, and 8×10^{-11} cm^3 sec^{-1}, respectively.

PACS numbers: 82.50.Et, 31.70.Hq, 31.50. + w

The kinetics of the C state of the XeF molecule are of interest both because of its close proximity to the B state previously made to lase[1] and because of recent observations[2-5] of laser action on the C-A transition in the 480–490-nm region. Previous measurements[6] of the XeF(C) state radiative lifetime and the quenching by XeF_2 were made by electron impact dissociation of XeF_2. This work reexamines the lifetime of XeF(C) and measures the quenching of the C state by numerous gases by the method of photodissociating XeF_2 in the presence of itself and quenching gases. The results reconfirm previous measurements of the XeF(C) state lifetime and quenching rate constant, indicating little effect from electrons in the previous measurements.

These measurements of lifetime and quenching of XeF(C) were made using the photolysis system shown in Fig. 1. This apparatus was very similar to the previous system used to measure lifetimes and quenching rate constants for XeF(B)[7,8] and KrF(B).[9,10] By increasing the x-ray shielding which isolates the electron beam and gas cell from the detector, it was possible to operate on a sufficiently sensitive scale that the 450–550-nm photons from XeF(C) state decay could be recorded reliably.

In operation the Febetron 706 produced a ~3-ns FWHM pulse of 600-keV electrons which passed through the foil of the Hewlett-Packard type 5515 e-beam tube. When these electrons passed into the gas cell containing 2000-Torr Ar and 20-Torr Cl_2, short ArCl pulses (175 nm) were produced which, as previously seen,[7,8] dissociated XeF_2 very rapidly into XeF(B), XeF(C), etc. The 450–550-nm photons from the XeF($C \rightarrow A$) decay were allowed to pass through a bandpass filter onto the photocathode of an F4018 photodiode, while the stronger XeF($B - X$) ultraviolet emission was rejected. The photodiode signal was recorded by photographing the display of the fast Tektronix 7904 oscilloscope.

To measure the XeF(C) state radiative lifetime and quenching rate constant, the XeF_2 pressure was varied from ~0.1 to 2 Torr. The oscillograms were manually digitized, plotted on a semilog scale to determine the decay time τ, and the decay rates τ^{-1} were plotted versus pressure. Since the measured decay rate τ^{-1} is given by

$$\tau^{-1} = \tau_r^{-1} + K_Q[XeF_2], \quad (1)$$

where τ_r^{-1} is the radiative lifetime, K_Q is the quenching rate constant, and [ ] denote particle densities (cm^{-3}), the graph slope is K_Q and the zero-pressure intercept is the radiative lifetime. From Fig. 2 the quenching rate constant K_Q is $(1.7 \pm 0.1)\times10^{-10}$ cm^3 sec^{-1} and the XeF(C) state lifetime is 95 ± 7 ns. Within experimental error these numbers agree very well with the 93 ± 5-ns lifetime and $(1.8 \pm 0.5)\times10^{-10}$ cm^3 sec^{-1} quenching rate constant determined previously by electron impact dissociation of XeF_2. This would confirm the assumption that electron

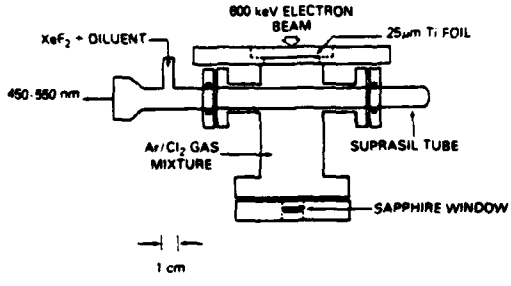

FIG. 1. Diagram of photolysis apparatus used to study XeF(C).

quenching of the XeF(C) state was very small in the previous experiment[6] and that electron mixing of the B and C states also was not important in that experiment since it did not result in a significantly faster decay from XeF(C). These numbers are in reasonable agreement with those of Black *et al.*[11] (100 ± 10 ns, 5×10^{-10} cm sec^{-1}), who studied XeF(C) by photodissociation of XeF_2 with synchrotron radiation.

In the above analysis, it is necessary that the dissociation of XeF_2 into XeF* and F be a small percentage of the total gas such that quenching, etc., by dissociation products is small. Further, when other quenching gases are added, such that

$$\tau^{-1} = \tau_r^{-1} + K_{XeF_2}[XeF_2] + K_Q[Q], \qquad (2)$$

then $[XeF_2]$ must be kept small enough that $K_{XeF_2}[XeF_2]$ is small compared to $K_Q[Q]$.

Measurement of the quenching of gases likely to be used in XeF($C-A$) lasers was carried out using a fixed pressure of XeF_2 of 0.1–0.5 Torr. Data were recorded and analyzed in a manner similar to the quenching analysis of XeF_2 above. A summary of the rate constants determined for the XeF(C) state as well as those previously determined for the B state[7,8] are given in Table I.

Studies of XeF(C) state quenching have been carried out both by Black *et al.*[11,12] and by Brashears and Setser.[13] Black *et al.* give rate constants only for N_2 (2.5×10^{-14} cm^3 sec^{-1}) and Ar (7×10^{-15} cm^3 sec^{-1}), but these values are significantly lower than determined here. While full details of that experiment are not yet available, a possible explanation is that additional quenching may take place due to photolysis products at low quenching-gas pressures. This would lead to a flatter rate-versus-pressure curve and a lower rate constant. Brashears and Setser[13] have studied B and C state quenching and B-C energy transfer using a steady-state technique. Comparison with their results is difficult because they used a C state lifetime of 150 ns in their calculations and give results in terms of the transfer rate constant. However, their results for B state quenching agree well with those of Table I and their implied C state quenching rate constant for He ($<2 \times 10^{-13}$ cm^3 sec^{-1}) agrees with the value determined here.

TABLE I. Quenching rate constants for XeF(B and C) by gas laser constituents.[a]

	XeF(B)[b]	XeF(C)
He	$(4.07 \pm 1.46) \times 10^{-13}$	$(1.2 \pm 0.2) \times 10^{-13}$
Ne	$(7.68 \pm 1.6) \times 10^{-13}$	$(3 \pm 0.1) \times 10^{-13}$
Ar	$(4.92 \pm 1.56) \times 10^{-12}$	$(9 \pm 0.1) \times 10^{-16}$
Xe	$(3.27 \pm 0.74) \times 10^{-11}$	$(1 \pm 0.5) \times 10^{-12}$
F_2	$(3.80 \pm 0.13) \times 10^{-10}$	$(8 \pm 0.2) \times 10^{-11}$
NF_3	$(2.8 \pm 0.15) \times 10^{-11}$	$(1.6 \pm 0.2) \times 10^{-13}$
XeF_2	$(2.56 \pm 0.32) \times 10^{-10}$	$(1.7 \pm 0.1) \times 10^{-10}$
N_2		$(4 \pm 0.4) \times 10^{-13}$

[a]All units are cm^3 sec^{-1}.
[b]References 7 and 8.

The uncertainty expressed in the C state quenching rate constants is the standard deviation of the data about the linear least-squares fit. In the case of xenon the data appeared to show a slight quadratic dependence, but a quadratic least-squares fit over the pressures used (700-Torr maximum) resulted in greater uncertainty about the fitted line than the linear fit.

In summary, the radiative lifetime of XeF(C) was determined by a photolysis experiment and found to agree very well with a previous measurement using electron impact dissociation. Quenching rate constants for XeF(C) have been presented for gases likely to be used in the XeF(C) state laser.

The author appreciates discussions of this problem with L.J. Palumbo.

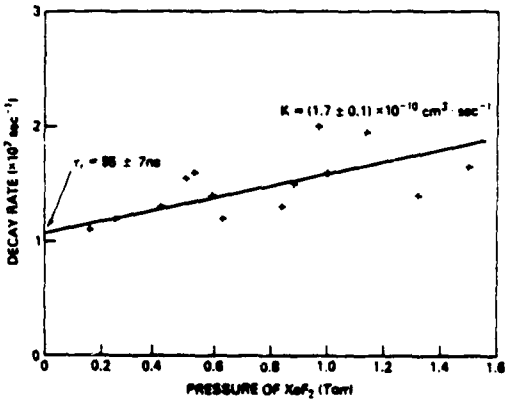

FIG. 2. Plot of XeF(C) fluorescent decay rate as a function of XeF_2 pressure. The zero-pressure intercept gives the radiative lifetime and the slope gives the rate constant.

[1]See *Excimer Lasers*, edited by C.K. Rhodes (Springer-Verlag, New York, 1979) and references therein.
[2]W.K. Bischel, H.H. Nakano, D.J. Eckstrom, R.M. Hill, D.L. Huestis, and D.C. Lorents, Appl. Phys. Lett. 34, 567 (1979).
[3]W.E. Ernst and F.K. Tittel, Appl. Phys. Lett. 35, 36 (1979).
[4]R. Burnham, Appl. Phys. Lett. 38, 48 (1979).
[5]C.H. Fisher, R.E. Center, G.J. Mullaney, and J.P. McDaniel, Appl. Phys. Lett. 35, 26 (1979).
[6]R.W. Waynant and J.G. Eden, IEEE J. Quantum Electron. 15, 61 (1979).
[7]J.G. Eden and R.W. Waynant, Opt. Lett. 2, 13 (1978).
[8]J.G. Eden and R.W. Waynant, J. Chem. Phys. 68, 2850 (1978).
[9]J.G. Eden, R.W. Waynant, S.K. Searles, and R. Burnham, Appl. Phys. Lett. 32, 733 (1978).
[10]J.G. Eden, R.W. Waynant, S.K. Searles, and R. Burnham, J. Appl. Phys. 49, 5368 (1978).
[11]G. Black, R. Sharpless, D.C. Lorents, R. Gutchek, T. Bonifield, D. Helms, and G.K. Walters, *Technical Digest Excimer Lasers* (Optical Society of America, Washington, D.C., 1979), Abstract TuA6.
[12]D.C. Lorents (private communication).
[13]H.C. Brashears, Jr., and D.W. Setser, Appl. Phys. Lett. 33, 821 (1978).

$Xe(^3P_2)$ + HCl(v=1): Vibrational Enhancement of XeCl* Formation

R. S. F. Chang
Laser Physics Branch
Optical Sciences Division
Naval Research Laboratory
Washington, D. C. 20375

Abstract

Formation of XeCl* by way of $Xe(^3P_2)$ + HCl reactions is slightly endothermic. In this work laser excitation of HCl(v=1) in the presence of $Xe(^3P_2)$ produced in a flowing afterglow apparatus allows direct observation of XeCl* fluorescence from $Xe(^3P_2)$ + HCl(v=1) reactions. The formation rate constant is determined to have a lower limit of 2×10^{-10} cm^3 sec^{-1}.

Introduction

Recently, efficient laser oscillation on the XeCl(B-X) transition at 308 nm has been reported.[1] HCl is commonly used as the chlorine donor in XeCl lasers because of no long-term degradation of laser performance and no ground state absorption at the laser wavelength with HCl. Fluorescence yield measurement[2] also indicates that the XeCl* is being formed efficiently via rare gas excitation by electron beam. However, the details of the formation kinetics are not well known. As in other rare gas halide lasers, both ionic and neutral formation channels have to be considered. The ion-ion Xe^+-Cl^- recombination reactions is assumed to be fast (10^{-7} cm^3 sec^{-1}) based on theoretical calculations[3] and gives unity branching ratio for XeCl* formation. On the other hand, experimental studies of neutral reactions between rare gas excited atoms and HCl have been reported. Due to the strong bond energy of HCl, the reaction of $Xe(^3P_2)$ and $(^3P_1)$ with HCl to form XeCl* is endothermic by about 1200 cm^{-1} and 200 cm^{-1} respectively. Setser and his coworkers[4] have observed no XeCl* emission in the quenching of $Xe(^3P_2)$ metastable or $Xe(^3P_1)$ resonance states by HCl even though the total quenching rate constant is large. The $Xe(^1P_1$ and $^3P_0)$ states are separated by about 1 eV from the lower $^3P_1$ and $^3P_2$ states and reaction with HCl to form XeCl* is energetically allowed. Recent work by Tang et al.[5] using synchrotron radiation to excite $Xe(^1P_1)$ found a small branching ratio for XeCl* formation. Thus, it would seem that exothermicity is not the only criteria.

HCl has a large cross section for vibrational excitation by electrons[6] and hence in the laser plasma a significant fraction of the HCl molecules is vibrationally excited. One important consequence of HCl vibrational excitation has already been observed by Allan and Wong[7] in the enhancement of dissociative attachment cross section. The large vibrational spacing of HCl molecule also makes it possible for HCl in v=1 level with E_v = 2886 cm^{-1} to overcome the endothermicity of XeCl* formation from $Xe(^3P_0)$ + HCl(v=0) i.e.,

$$Xe(^3P_2) + HCl(v=1) \xrightarrow{k_f} XeCl^*(B,C) + H \qquad (1)$$

$$\xrightarrow{k_q} \text{other products} \qquad (2)$$

In this paper we present experimental data that indicates vibration excitation in HCl can influence the reaction pathway of $Xe(^3P_2)$ + HCl. HCl was

vibrationally excited by a pulsed HCl chemical laser in the presence of $Xe(^3P_2)$ in a flowing afterglow apparatus and XeCl* fluorescence was observed. The formation rate constant of XeCl* from $Xe(^3P_2)$ + HCl(v=1) was determined to have a lower limit of 2×10^{-10} cm^3 sec^{-1}.

Experimental

The experimental apparatus is shown in Fig. 1. Xe metastable atoms were generated[8] by flowing Ar/Xe through a hollow cathode discharge in a flowing afterglow apparatus slightly modified for monitoring laser induced fluorescence. Less than 0.1% of research grade Xe was added to a purified argon flow before the discharge. This produced mainly $Xe(^3P_2)$ downstream from the discharge. HCl diluted in argon was admitted through a reagent inlet and mixed in concentrically with main flow. The flow then entered the aluminum fluorescence cell fitted with a pair of CaF_2 Brewster windows for IR laser radiation and another pair of CaF_2 side windows for monitoring laser induced fluorescence at right angle to the plane defined by the flow direction and the laser radiation. The cell was pumped by a 500 l/min pump.

Vibrationally excited HCl was generated by excitation with a transverse electric discharge chemical laser using a H_2/Cl_2 gas mixture. The laser was either operated in free-running mode or line-tuned to a certain 1P(J) transition with a grating. The laser pulsed at 1-2 pps with a pulse duration of about 2 μsec. Approximately 23% of the output was in v=1→0 P branch transitions, 47% in v=2→1 and 30% in v=3→2 bands. The laser pulse energy was 8 mJ as measured by a Gen-Tec ED-200 Joulemeter. The pulse energy of the grating-tuned 1P(5) laser line was less than 1 mJ. The XeCl uv fluorescence was detected with an RCA 1P28 photomultiplier through a uv filter centered at 310 nm with a FWHM bandwidth of 140 nm. Even with careful shielding of light from the hollow cathode discharge, enough light was reflected into the cell and observed by the PMT as a DC signal. Therefore, the tube was protected by a time-controlled shutter which was triggered to open for a period of a few msec every time the IR laser was fired. The timing of the shutter was such that it was fully open when the laser pulse arrived and remained open until the uv fluorescence pulse was completely gone. Attempts to monitor the laser induced HCl IR fluorescence failed despite repeated efforts with a highly sensitive IR detection system. This will be explained further in the results section. The IR detection system consisted of a CaF_2 f/1 lens to

collect IR emission from the center of the cell and focus onto the liquid N_2 cooled InSb detector with an IR filter to transmit only the v=1 → v=0 transitions of the R branch of HCl. The cold gas cell with a 5 cm path length was evacuated for the present use. A positive argon flow was admitted to the cell near each Brewster window to prevent HCl from being trapped in the region between the window and the mixing zone. The temperature in these experiments was ambient (300°K) and the temperature rise due to V-R, T relaxation of HCl excitation created by the laser was insignificant.

The Xe metastable atom concentrations were measured using atomic absorption technique.[9] This method has been described in great detail elsewhere.[10] Briefly, the 8819 Å line of the Xe($^3P_2$-6p[5/2]$_2$) transition from a Pen-Ray lamp was selected for the absorption measurement. A triple pass of light through the reactor was set up to increase absorption for the Xe line by the Xe($^3P_2$) present in the flow. The Xe($^3P_2$) concentrations thus determined under a wide range of conditions varied from 10^9-10^{10} cm^{-3} which is typical for this method of Xe($^3P_2$) generation. The main flow of argon was measured with a Matheson flowmeter (#603) originally calibrated for air at 70°F and at atmospheric pressure. To determine the actual flow the calibration was corrected for the change of gas density and viscosity. The flow rate was independently checked by monitoring the pressure rise in a 15 liter volume as a function of time. Flow rates determined by the two methods agreed to within 10%. In general the exhaust valve to the vacuum pump was fully opened and the flow rate as well as pressure in the reaction were controlled by actual pressure in the flow tube and a needle valve placed after the flowmeter. The reagent flow being much slower was measured by the rate of pressure rise in a small standard volume. Main flow rate ranged from 10^{-1}-10^{-2} mole/min while the reagent flow rate was more like 10^{-4}-10^{-5} mole/min. The bulk-flow velocity in the reactor was in the 1-2 x 10^3 cm/sec range. Matheson purity grade (99.9995%) argon was passed through a liquid N_2 cooled trap filled with molecular sieve before flowing into the discharge and Xe was of Matheson research grade. The HCl (Air Products electronic grade) was purified by degassing at 77°K followed by distillation from a reservoir at -120°C to one at 77°K. The Cl_2 (Matheson high purity) was degassed at 77°K and collected over a trap at dry ice temperature.

Results and Discussion

The HCl chemical laser excites a sufficient number of HCl molecules for

observation of XeCl* fluorescence from the reaction of Xe* + HCl(v). Figure 2 shows the oscilloscope photographs of XeCl uv fluorescence signal under different laser pumping conditions. The lower trace in each photograph shows the laser excitation pulse as a sharp spike on the 100 μs/div time scale. The decay of the fluorescence signals (top and middle) looks much the same except the signal was stronger in the case of multiline excitation. There is a delay of about 40 μs between the laser pulse and the fluorescence signal peak. This is probably associated with the mixing time of the reagent flow with the main flow. The decay time of the uv signal was controlled by the reagent flow only. The bottom photograph in Fig. 2 shows the decay time was significantly lengthened when the HCl concentration in the mixing zone was lowered. The latter could be accomplished by changing the regulating needle valve setting, the dilution factor of HCl in argon, or partially closing the main valve to the vacuum pump.

The power dependence of the peak signal level was investigated to look for evidence of contribution from HCl(v>1) levels. Fine mesh copper screens were used to attenuate the laser beam. The transmission of these screens were measured both individually and in combination. With the laser tuned to excite the (v=0, J=5, v=1, J=4) transition of HCl a linear power dependence of the signal was observed as illustrated in Fig. 3a. This clearly indicates that XeCl* was formed from Xe* + HCl (v=1) and that the laser was not saturating the infrared transition. Contribution from HCl(v=2) was ruled out because the HCl V-V laddening time (via process 6 in Table 1) would be on the order of msec, much longer than the signal risetime here. Secondly, the signal would have a quadratic power dependence. When the laser was operated in free running condition, sequential absorption of a 1P(J) and a 2P(J-1) photons by a HCl molecule could result in v=2 excitation in addition to the V-V pumping. Quadratic power dependence is expected for reaction out of v=2 level to form XeCl* via either vibrational excitation method. However, a linear dependence was observed for the multiline excitation and no laser saturation effect was apparent (see Fig. 3b). The lack of formation of HCl(v=2) was most likely due to the low excitation of HCl(v=1) and the usual poor overlap in time of the lasing 3-2, 2-1 and 1-0 transitions. Hence, we can conclude that little or no HCl(v=2) were formed in our experiments and that XeCl* was the product emission of Xe* + HCl(v=1).

In order to understand the pressure and time dependence of the observed XeCl* fluorescence one must look to the kinetics of the excited species present namely XeCl*, HCl(v=1) and Xe*. Table I summarizes the rates of all the processes relevant to the present experiment. The rate equations for the three excited species are written as follows:

$$\frac{d}{dt}[Xe^*] = -\ k_1[HCl] + (k_f + k_q)\ [HCl(1)]\ \ [Xe^*] \tag{3}$$

$$\frac{d}{dt}[HCl(1) = R_{op} -\ k_p + \tau^{-1}_{HCl(1)}\ + (k_f + k_q)[Xe^*] + k_5[HCl]\ \ [HCl(1)] \tag{4}$$

$$\frac{d}{dt}[XeCl^*] = k_f[Xe^*][HCl(1)] - \tau^{-1}_{XeCl^*}\ [XeCl^*] \tag{5}$$

The loss terms are arranged in such a way to indicate their relative importance under our experimental conditions. Loss terms that are substantially smaller than the rest are deleted to simplify the equations. Typical specie concentrations in the reactor were: Ar (0.6-2.5 x 10^{17} atoms/cm^3), Xe (10^{13} atoms/cm^3), Xe* (10^9-10^{10} atoms/cm^3), HCl (10^{12}-10^{13} molecules/cm^3) and HCl (1) (10^{11}-10^{12} molecules/cm^3).

For Xe metastable quenching, the sum of $(k_f + k_q)$ represents the total quenching rate constant of Xe* by HCl(v=1) while k_1 is that by HCl(v=0). If we assume $k_1/(k_f + k_q) \sim 1$, then the first term is larger than the second term by a factor of [HCl]/[HCl(1)] which is typically < 0.1 in our case. The above assumption also implies that the vibrational excitation of HCl does not change the magnitude of the total quenching rate constant of Xe* but rather the branching ratio for XeCl* formation. For the vibration deactivation of HCl(v=1), R_{op} is the optical pumping term which is zero after 2 μsec. The loss term is dominated by k_p, the removal rate of HCl(v=1) by the fast flow out of the observation zone. This k_p term was cancelled out in eqn. (3) for Xe*. Since the laser excites at most 10% of the HCl per pulse, secondary reactions involving Cl and H atoms are important and are ignored. Loss of XeCl* is completely radiative with no collisional quenching and any XeCl* formed would emit a photon before leaving the observation zone. Such simplification leads to:

$$I_{XeCl^*} = k_f[Xe^*]_o[HCl(1)]_o \, e^{-(k_p + k_1[HCl])t} \qquad (6)$$

This expression for I_{XeCl^*} correctly predicts the observed amplitude and decay time characteristic of the XeCl* fluorescence in that (1) the peak signal intensity is a linear function of the reactant concentrations and (2) the XeCl* decay time decreases with increase in flow velocity and the HCl concentration or vise versa.

The XeCl* fluorescence decay rate was measured as a function of HCl pressure in the mixing zone. The HCl pressure was calculated from the Ar/HCl dilution factor, the reagent flow, the argon main flow and the total pressure in the reactor. The results shown in Fig. 4 give a linear plot with a slope of 2.8×10^{-10} cm^3/sec and a zero pressure intercept of about 2×10^3 sec^{-1}. The rate constant is a factor 2 smaller than that reported by Setser and his coworkers[4a] for quenching of Xe* by HCl. The decay rate of 2×10^3 sec^{-1} for XeCl* as HCl pressure approaches zero can be explained by the flow removal rate of HCl(1). The bulk flow velocity was determined to be 1.7×10^3 cm/sec in these measurements and the dimension of the observation zone in the flow direction was less than 2 cm.

Spectroscopic transitions for XeCl that have been identified are D-X, B-X, B-A and C-A. Since the D state lies about 1.5 eV above the closely spaced B and C states,[4,29,30] formation of D state is not possible from $Xe(^3P_2)$ + HCl(v<5) reactions. No attempt was made to monitor the D-X transition at 236 nm. The uv filter with its broad bandpass would transmit the entire (B-X) transition peaked at 308 nm and the blue wing of the broad (C-A) transition. A plate glass filter (uv cut off at 325 nm) replaced the uv filter to look at only the (C-A) band fluorescence intensity. The decay of the (C-A) fluorescence followed that of the uv signal closely. Comparison of XeCl* fluorescence signal intensities using the two different filters gave an emission ratio of $I_B/I_C = 4$ at a pressure of 3 torr of mainly argon. No correction was made for the minor (B-A) contribution to the (C-A) fluorescence intensity.

The ratio I_B/I_C if determined under conditions which do not permit mixing or quenching of the electron excited states is a direct measure of the ratio of rate constants k_B/k_C. The frequency with which a XeCl* molecule will collide with Ar is about 9×10^6 sec^{-1} per torr of argon. At a few torr, the

time between collisions is longer than the radiative lifetime[27] of the B state (τ = 11 nsec) but shorter than that of the C state (τ = 120 nsec).[27] Vibrational relaxation of the C state is possible if relaxation rate is close to the gas kinetic rate. Collisional transfer rate from C to B on the other hand depends strongly on the vibrational level of XeCl* and k_{C-B} in Ar can vary from 6 x 10^{-11} cm^3 sec^{-1} for high v to 1.2 x 10^{-11} cm^3 sec^{-1} for a 300°K Boltzmann distribution.[4] With reaction (1) being slightly exothermic, high vibrational levels (v>7) of XeCl* are not expected to be excited. Thus a k_{C-B} in the low range of 10^{-11} cm^3 sec^{-1} is probably more appropriate and at 3 torr the C-B transfer rate is slow compared to the C state radiative decay. Based on this argument, the XeCl* B and C states formed from reaction (1) would not be well coupled and $I_B/I_C = k_B/k_C = 4$. Interestingly, this is very different from the values of k_B/k_C (1.0 to 1.7) determined for other ground state chlorine donors in quenching of Xe*.[4a] The XeCl(B-X) emission spectra from Xe* + HCl(1) reaction would also be narrower than that from Xe* + Cl_2, for example, at the same pressure. Unfortunately, the combination of low PMT signal and slow repetition rate of the HCl laser made it very difficult if not impossible to record the XeCl* spectra.

The reaction of Xe($^3P_2$) with Cl_2 was used as the reference reaction for assignment of rate constant to exit channel quenching of Xe($^3P_2$) by HCl(v=1) forming XeCl*. The rate constant for

$$Xe(^3P_2) + Cl_2 \xrightarrow{k_{Cl_2}} XeCl^* + Cl \qquad (7)$$

has been measured[4a] to be 7.2 x 10^{-10} cm^3/sec at 300°K. With no quenching of XeCl* other than radiative decay, k_f can be obtained by comparing the total emission intensities:

$$\frac{I^{HCl(1)}_{XeCl^*}}{I^{Cl_2}_{XeCl^*}} = \frac{k_f[Xe(^3P_2)][HCl(1)]}{k_{Cl_2}[Xe(^3P_2)][Cl_2]} \qquad (8)$$

$$\text{or } k_f = k_{Cl_2} \times \frac{I^{HCl(1)}_{XeCl^*}}{I^{Cl_2}_{XeCl^*}} \times \frac{[Cl_2]}{[HCl]f_v} \quad \text{where } f_v = [HCl(1)]/[HCl] \qquad (9)$$

To assure that the concentration of Xe($^3P_2$) remained constant during this

measurement, the flow from the two reservoirs containing Cl_2 and HCl diluted in argon to 1 atm, was regulated by a single metering valve and the main flow was not disturbed as the reagent flow was switched from one reservoir to the other. Ratio of $\frac{[Cl_2]}{[HCl]}$ could be accurately determined by the dilution factor in preparing the Ar/Cl_2 and Ar/HCl mixtures. The XeCl* emission from reaction (7) was observed as a continuous signal gated by the time-controlled shutter. This D.C. signal was compared to the peak XeCl* fluorescence from the Xe* + HCl (v=1) reaction using multiline laser excitation with 1.4 mJ incident energy.

With the flowing afterglow technique the conditions are such that the reagent flow (concentration) be kept low so that the product emission intensity varies linearly with the reagent flow and the metastable concentration is not significantly reduced. With HCl pressure in the reactor typically below 1 micron, absorption of the laser radiation in a single pass through the cell and laser induced fluorescence from vibrationally excited HCl molecules were therefore understandably small and difficult to detect. In order to determine f_v, calculations were made to estimate the amount of absorption under the best of conditions. Absorption coefficient, α_J (in units of cm^{-1} $torr^{-1}$), was calculated at the line center of each 1P(J) lasing transition assuming Doppler broadening and T = 300°K. For low absorption, total number of laser photons absorbed = $\sum_J I_J^{1-0} \alpha_J p\ell$ where I_J^{1-0} is the number of photons per laser pulse in the 1P(J) transition, p is the HCl pressure and ℓ is the absorption length (1.5). The excitation volume was defined by the product of the area of the laser beam (1.5 cm^2) and ℓ. Since the total number of HCl(v=1) produced must equal the number of laser photons absorbed, this gave a calculated value of $f_v = 0.07$. It is important to note that the latter represents an upper limit of f_v. With $f_v \leq 0.07$ in eqn. (9) the rate constant k_f deduced has a lower limit of 2×10^{-10} cm^3 sec^{-1}.

Conclusion

Pulsed chemical laser excitation of the vibrational manifold of ground state HCl molecules in the presence of $Xe(^3P_2)$ metastable atoms produced XeCl* in an otherwise endothermic reaction. In this study only the first vibrational level of HCl was excited. The observed XeCl* fluorescence can be explained by a simple kinetic scheme. Although the total quenching rate constant of $Xe(^3P_2)$ by HCl(v=1) was not measured, branching ratio for XeCl*

formation must be quite large with $k_f \geq 2 \times 10^{-10}$ cm^3 sec^{-1}. It is somewhat surprising to find such efficient XeCl* formation out of the HCl(v=1) level. It is tempting to suggest the reaction mechanism is again the "harpooning" type as in the Xe* + Cl_2 case[4a] except here vibrational excitation is required to enhance the dissociative attachment of HCl. It would clearly be of interest to investigate the Xe($^3P_2$) + HCl reaction as a function of vibrational excitation in HCl. In particular, it is interesting to see if any further enhancement occurs for v>1.

Acknowledgement

The author wishes to thank Dr. N. Djeu and Professor D. W. Setser for their helpful discussions and comments on the manuscript. He also wishes to thank Dr. M. C. Lin and Dr. J. Butler for the use of their chemical laser and infrared detection system. The able technical assistance of K. Tayman and D. M. Shores is also appreciated. This work was sponsored by the Defense Advanced Research Projects Agency, DARPA Order

References

1. (a) L. F. Champagne, Appl. Phys. Lett. 33, 523 (1978); (b) D. E. Roth, J. B. West and M. L. Bhaumik, IEEE J. Quant. Elect. QE-15, 314 (1979); (c) W. L. Nighan and R. T. Brown, Appl. Phys. Lett. 36, 498 (1980).
2. T. G. Finn, R. S. F. Chang, L. J. Palumbo and L. F. Champagne, Appl. Phys. Lett. 36, 789 (1980).
3. (a) J. M. Wadehra and J. N. Bardsley, Appl. Phys. Lett. 32, 76 (1978); (b) M. R. Flannery and T. P. Yang, Appl. Phys. Lett. 32, 327 (1978); (c) M. R. Flannery and T. P. Yang, Appl. Phys. Lett. 32, 356 (1978).
4. (a) J. H. Kolts, J. E. Velazco and D. W. Setser, J. Chem. Phys. 71, 1247 (1979); (b) H. C. Brashears, Jr. and D. W. Setser, J. Phys. Chem. 84, 226 (1980).
5. K. Y. Tang, D. C. Lorents, R. L. Sharpless, D. L. Huestis, D. Helms, M. Durrett and G. K. Walters, presented at the 33rd Gaseous Electronics Conference, Norman, OK, October 1980 (unpublished).
6. K. Rohr and F. Linder, J. Phys. B9, 2521 (1976).
7. M. Allan and S. F. Wong, J. Chem. Phys. 74, 1687 (1981).
8. J. H. Kolts and D. W. Setser, "Electronically Excited Long-Lived States of Atoms and Diatomic Molecules in Flow Systems," in Reactive Intermediates in the Gas Phase, edited by D. W. Setser (Academic Press, 1979).
9. A. C. G. Mitchell and M. W. Zemansky, Resonance Radiation and Excited Atoms (Cambridge University, London, 1971).
10. J. E. Velazco, J. H. Kolts and D. W. Setser, J. Chem. Phys. 65, 3468 (1976) and references cited within.
11. R. E. Gleason, T. D. Bonifield, J. W. Keto and G. K. Walters, J. Chem. Phys. 66, 1589 (1977).
12. P. R. Timpson and J. M. Anderson, Can. J. Phys. 48, 1817 (1970).
13. W. Wieme, J. Phys. B7, 850 (1978).
14. A. Barbet, N. Sadeghi and J. C. Pebay-Peyroula, J. Phys. B8, 1776 (1975).
15. J. K. Cashion and J. C. Polanyi, Proc. Roy. Soc. A 258, 529 (1960).

16. H. L. Chen and C. B. Moore, J. Chem. Phys. 54, 4072 (1971).
17. I. Burak, Y. Norter, A. M. Ronn and A. Szoke, Chem. Phys. Lett. 17, 345 (1972).
18. S. R. Leone and C. B. Moore, Chem. Phys. Lett. 19, 340 (1973).
19. B. M. Hopkins and H. L. Chen, J. Chem. Phys. 57, 3816 (1972).
20. B. A. Ridley and I. W. M. Smith, J. Chem. Soc. Faraday Trans. II, 1231 (1972).
21. D. Arnoldi and J. Wolfrum, Chem. Phys. Lett. 24, 234 (1974).
22. J. F. Bott and R. F. Heidner, III, J. Chem. Phys. 64, 1544 (1976).
23. (a) N. C. Craig and C. B. Moore, J. Phys. Chem. 75, 1622 (1971); (b) R. G. MacDonald, C. B. Moore, I. W. M. Smith and F. J. Wodarczyk, J. Chem. Phys. 62, 2934 (1975).
24. R. D. Brown, G. P. Glass, and I. W. M. Smith, J. Chem. Soc. Faraday Trans. II 71, 1963 (1975).
25. Z. Karny and B. Katz, Chem. Phys. Lett. 38, 382 (1976).
26. M. Kneba and J. Wolfrum, Ber. Bunsenges, Phys. Chem. 82, 1234 (1978); J. Phys. Chem. 83, 69 (1979).
27. P. J. Hay and T. H. Dunning, Jr., J. Chem. Phys. 69, 2209 (1978).
28. C. H. Fisher, R. E. Center and J. P. McDaniel, presented at 32nd Annual Gaseous Electronics Conference, Pittsburgh, PA, October 1979 (unpublished).
29. J. Tellinghuisen and M. R. McKeever, Chem. Phys. Lett. 72, 94 (1980).
30. J. Bokor and C. K. Rhodes, J. Chem. Phys. 73, 2626 (1980).

TABLE 1. Quenching processes involving $Xe(^3P_2)$, HCl(v=1) and XeCl*.

Process	Rate Constant (in units of $cm^3\ sec^{-1}$)	Reference
$Xe(^3P_2)$ Quenching		
1. $Xe^* + HCl(v=0) \rightarrow$ products	5.6×10^{-10}	4a
2. $Xe^* + Ar \rightarrow$ products	0.4×10^{-15}	11
3. $Xe^* + Xe \rightarrow$ products	3.7×10^{-15}	12
	3.5×10^{-15}	13
	2.3×10^{-15}	14
HCl(v=1) Vibrational Deactivation		
4. $HCl(1) \rightarrow HCl(0) + h\nu$	$\tau^{-1}_{HCl(1)} = 33\ sec^{-1}$	15
5. $HCl(1) + HCl(0) \rightarrow 2HCl(v)$	2.4×10^{-14}	16
6. $HCl(1) + HCl(1) \rightarrow HCl(2) + HCl(0)$	2.8×10^{-12}	17
	5.1×10^{-12}	18
	4.3×10^{-12}	19
	2.3×10^{-12}	20
7. $HCl(1) + Ar \rightarrow HCl(0) + Ar$	$\leq 3.1 \times 10^{-17}$	16
8. $HCl(1) + Xe \rightarrow HCl(0) + Xe$	$\leq 3.1 \times 10^{-17}$	16
9. $HCl(1) + H \rightarrow HCl(0) + H$	6.5×10^{-12}	21
	7.6×10^{-12}	22

TABLE 1. (continued)

10. $HCl(1) + Cl \rightarrow HCl(0) + Cl$	8.8×10^{-12}	23
	9.3×10^{-12}	24
	7.0×10^{-12}	25
	6.1×10^{-12}	26
XeCl* Quenching		
11. $XeCl^* \rightarrow XeCl + h\nu$	$\tau^{-1} = 9.09 \times 10^{7}\ sec^{-1}$	27
	$\tau^{-1}_{XeCl^*} \quad 6.25 \times 10^{7}\ sec^{-1}$	28
12. $XeCl^* + Ar \rightarrow$	5×10^{-13}	28
13. $XeCl^* + Xe \rightarrow$	1×10^{-11}	28
	3.2×10^{-11}	2
14. $XeCl^* + HCl \rightarrow$	8×10^{-10}	28
	1.4×10^{-9}	2

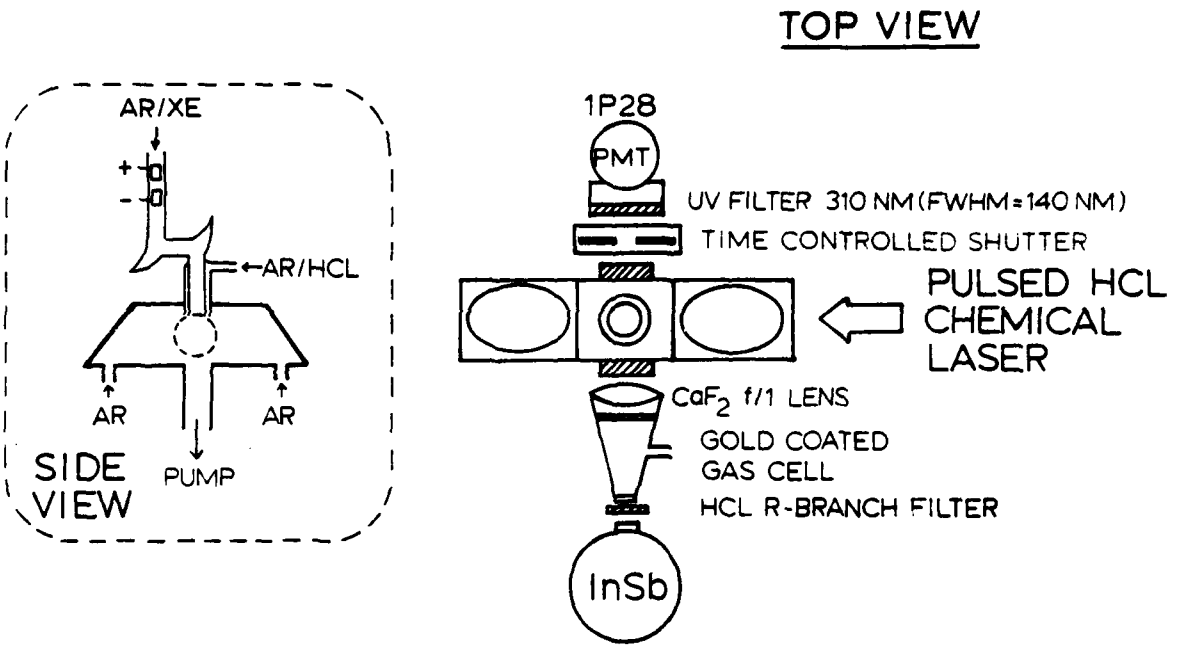

Fig. 1 - Experimental apparatus for the Xe* + HCl(v=1) studies

$$Xe(^3P_2) + HCl(v) \longrightarrow XeCl^* + H$$

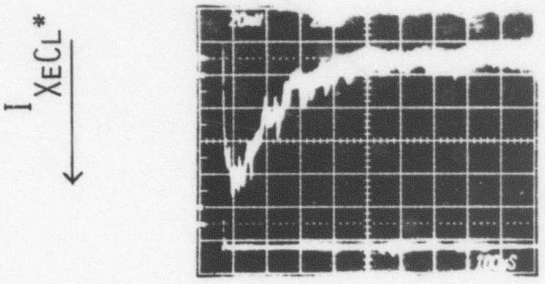

HCL LASER LINE TUNED TO $P_{1-0}(5)$ TRANSITION

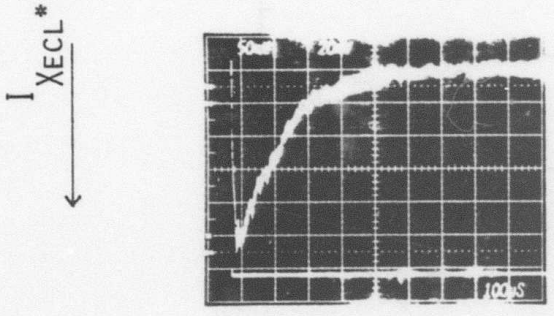

HCL LASER FREE RUNNING

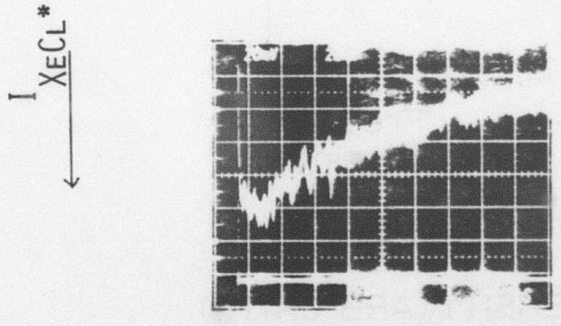

HCL LASER FREE RUNNING
HCL CONC. IN MIXING ZONE LOWERED

Fig. 2 - Oscilloscope photographs of XeCl* fluorescence from $Xe(^3P_2)$ + HCl(v) reaction. The bottom trace in each picture shows the laser excitation pulse as a spike. The HCl laser was line-tuned to 1P(5) transition in top and operated in free running in middle and bottom. The reagent flow Ar/HCl was the same in top and middle but much smaller in bottom. Time scale: 100 μs per div. P_{Ar} = 3.0 torr.

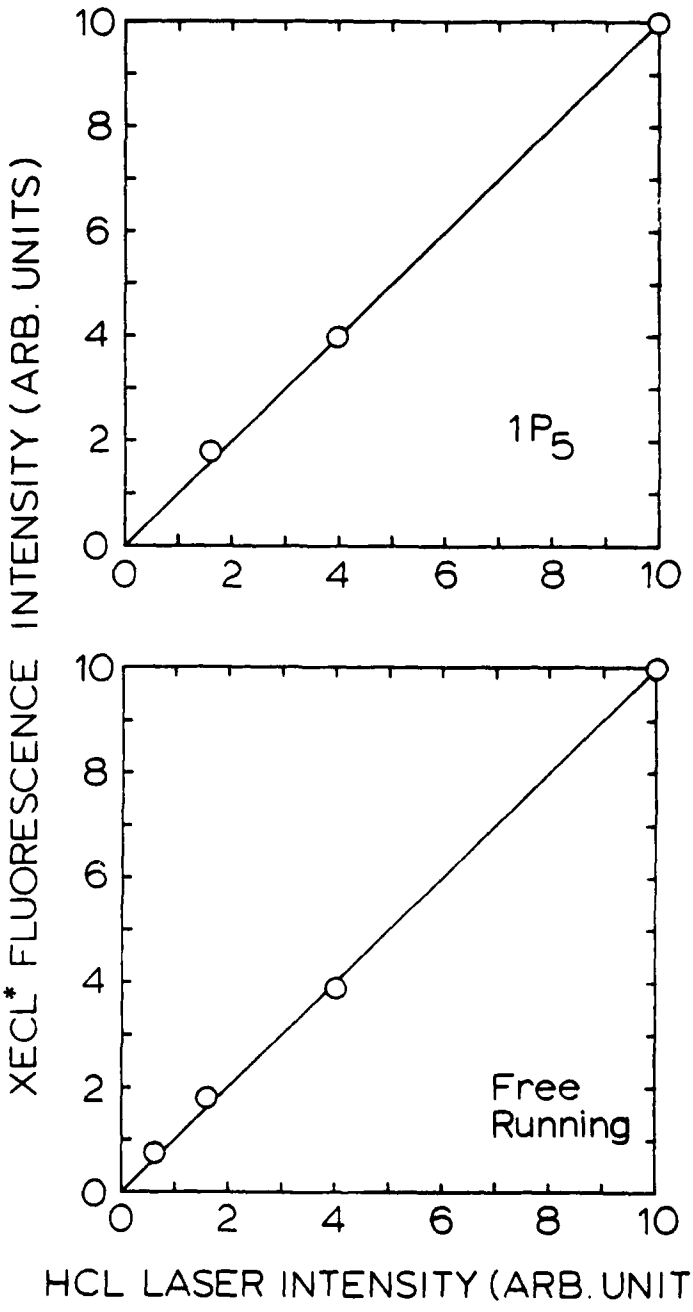

Fig. 3 - XeCl* fluorescence intensity as a function of HCl laser intensity (a) line-tuned 1P(5) and (b) free running. The curved lines describe quadratic laser power dependency.

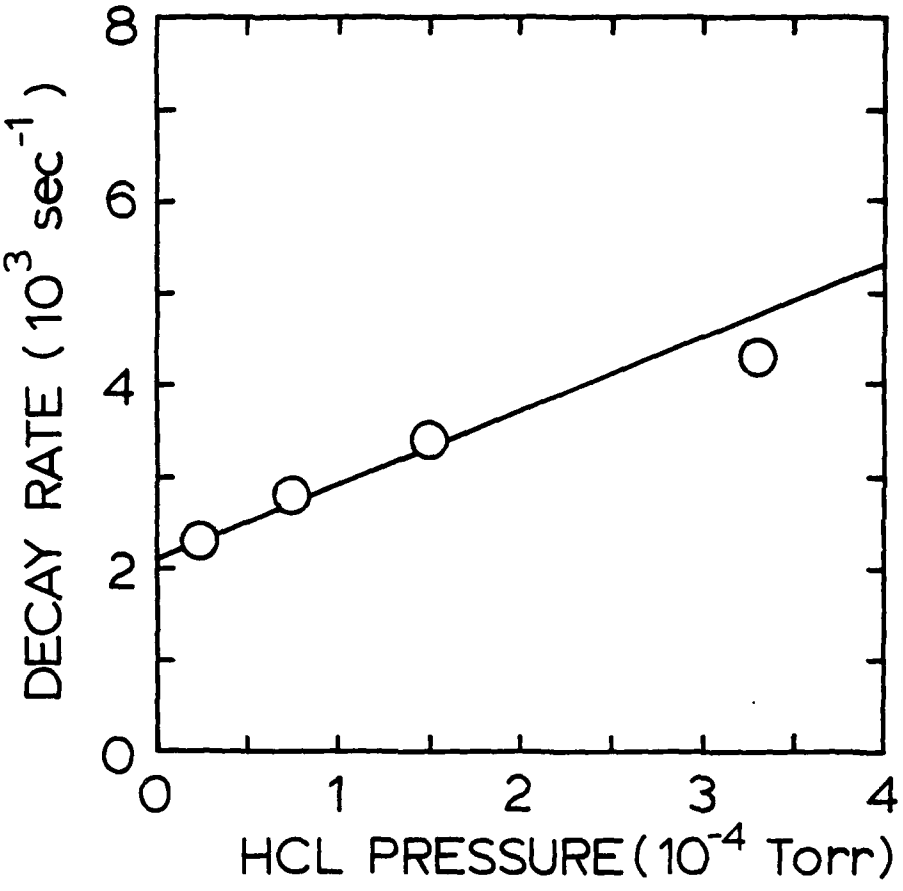

Fig. 4 - Observed XeCl* fluorescence decay rates as a function of HCl pressure in the reactor. Total reactor pressure was 2.6 torr (mainly Ar).

Collisional Quenching of Pb $6p^2\ ^3P_1$ and $6p^2\ ^3P_2$ Metastables By Ground State Pb Atoms

by

C. Reiser,* N. Djeu and R. Burnham
Laser Physics Branch, Optical Sciences Division
Naval Research Laboratory, Washington, D. C. 20375

ABSTRACT

Collisional quenching of the two lowest Pb atom metastable levels, $6p^2\ ^3P_1$ and $6p^2\ ^3P_2$, has been studied at Pb vapor densities of 1-20 x 10^{16} cm^{-3}. The metastable atoms were created in a heat pipe oven by stimulated Raman scattering using an XeCl laser pump. Their subsequent decay was then probed with tunable, single-frequency UV on the 266.3 and 261.4 nm Pb resonance lines. The observed rate constants are 2.0 x 10^{-13} cm^3 sec^{-1} for $^3P_1$ and 3.2 x 10^{-13} cm^3 sec^{-1} for $^3P_2$.

*NRC-NRL Postdoctoral Fellow

I. INTRODUCTION

Kinetic spectroscopy of the metastable states of gaseous lead atoms were first accomplished[1,2] by photographic detection of sensitized explosions containing tetraethyl lead, $PbEt_4$, in its relevance to antiknock effects in the internal combustion engine. In these experiments, flash photolysis initiated combustion in various gaseous mixtures containing $PbEt_4$ plus inert gases, in which the Pb resonance lines appeared immediately after initiation and decayed "extremely rapidly."[1] Using a similar flash photolysis technique in later investigations,[3,4] atoms in the spin-orbit split $6p^2\ ^3P_1$ metastable states were prepared at low concentrations in a wide variety of reactive and inert gases. The decay of these populations was typically monitored by resonance radiation from a spectroscopic lamp, and collisional deactivation rates were recovered[5] for temperatures up to 600°K. Processes involving E↔V and E↔T energy transfer were found to dominate the kinetics for the unreactive collision partners under the conditions used.

Recent progress in sustaining discharges in high temperatures, high Pb-vapor pressure columns has produced laser action on many atomic Pb transitions,[6,7] including some terminating on the $6p^2$ metastable states. Depopulation of the lower laser level proceeds by a combination of charge exchange[7] with rare gas ions, and by quenching via collisions with electrons and other Pb atoms. The latter phenomenon, quenching by Pb atoms themselves, had not been explored in the flash photolysis work because the Pb density was too low. Better understanding of the Pb laser requires kinetic information at Pb atom densities in excess of the vapor pressure of $PbEt_4$, so that the effects of collisions with ground state $6p^2\ ^3P_0$ atoms can be included.

Our interest in the Pb metastable states stems from earlier work[8,9] on the conversion of XeCl excimer laser output at 308 nm to the visible region at 459 nm by resonantly enhanced Stimulated Raman Scattering (SRS) in Pb vapor. This wavelength falls in the seawater blue-green transmission window, and the overall laser-Raman converter efficiency can reach a few percent.[10] SRS in Pb vapor can be easily accomplished, typically by weakly focusing the output of a discharge-pumped XeCl laser into a Pb heat pipe oven at approximately 1100°C, at which the Pb vapor pressure is 5 Torr. As shown in Fig. 1, the Raman process takes atoms from the ground state to the $^3P_2$ state, and is resonantly enhanced by the proximity of the $7s\ ^3P_1^0$ state to the virtual Raman level. For

repetitive performance, the metastables must be quenched to the ground state, hence the overall repetition rate of the laser-Raman converter system is ultimately determined by the $6p^2\ ^3P_2$ quenching rate. As for the Pb laser, detailed understanding of the Pb Raman converter necessitates knowledge of the kinetics of the Pb metastable levels in the presence of much higher Pb atom densities than have previously been used in kinetic studies. In this paper we present quenching data for both metastable levels under conditions where quenching by Pb atoms is the dominant method of relaxation, using an apparatus much different from those used in previous studies.

II. EXPERIMENTAL

Schematically the apparatus can be divided into two parts: (1) the method of creating a population of metastables and (2) the production and detection of light for probing this transient population. We employed the SRS process itself to create metastable atoms, because a large number of metastables can be produced by an excimer laser pulse in a time very much shorter than the expected decay times of the metastables. The XeCl laser we employed was of similar construction to others[11] used in this laboratory, being of the UV-preionized, transverse electric discharge variety. It typically delivered 10-20 mJ per pulse at 1 Hz with an unstable resonator cavity. The output coupler-lens focused the vertical stripe shaped output into a Pb heat pipe oven 1 m from the coupler. The vacuum-insulated oven was resistively heated by a dc supply to temperatures close to 1200°C. The heat pipe itself consisted of a 2 cm o.d. alumina ceramic tube with a 15 cm long stainless steel screen centered in the tube serving as a wick. Stainless steel, O-ring sealed flanges closed the tube ends and held Suprasil windows perpendicular to the tube axis. Buffer gas (Ar or He) was admitted through a vacuum fitting on one of the flanges before heating, typically to 150 Torr. The center of the heat pipe was placed at the focus of the excimer laser output so that the diverging 308 nm pump and the 459 nm Stokes beams generated therein could be collimated with a single 30 cm focal length quartz lens at the rear window of the oven, as shown schematically in Fig. 2. When the collimating lens was properly placed, the collinear pump and Stokes beams were approximately 3 x 5 mm in cross section and remained so after traveling several meters.

The collinear pumps passed through a probe oven very similar to the first oven, except that the tube of the probe oven was 2.2 cm o.d. and its flanges

held the windows at a 15^{o} angle to the tube axis. This vacuum oven was resistively heated with alternating current. The temperature of the inside of the tube was read with a MicroOptical Pyrometer from the Pyrometer Instrument Company by sighting through one window at the glowing portion of the tube. Buffer gas pressure was read from a 0-800 Torr Wallace & Tiernan gauge, and was always much higher than the vapor pressure of Pb at the middle of the tube to prevent diffusion of metastables out of the probing beam. The density of Pb atoms in the vapor phase was calculated from the tube temperature using well known[12] vapor pressure data. The validity of the assumption that the vapor temperature is in equilibrium with the tube walls will be discussed below.

The apparatus which produced the probe radiation was located on a separate optical table, in a configuration similar to that employed earlier.[13] A Spectra-Physics Model 171 Ar^{+} laser was constrained to a single longitudinal mode by an intracavity etalon, and produced 6.2 W at 488 nm. About 1 W was split from this beam, and the rest pumped a Spectra-Physics Model 375 electronically tunable dye laser utilizing two intracavity etalons for single-mode operation using either Rhodamine 6G or Rhodamine 110 dyes. The 30 mW output was collinearly combined with the 1 W 488 nm beam on a dielectric-coated beamsplitter and both were focused with an achromatic lens into a 5 cm length of KDP crystal cut 77^{o} to its optical axis. The KDP incidence angle was adjusted to achieve nominal phase matching for mixing the two visible beams to produce the sum frequency in the 260 nm region.

After emerging from the KDP crystal, the few microwatts of UV probe beam was collimated to approximately the same cross section as the pump beams. The visible beams were filtered off. With the help of movable irises, the probe beam was made to overlap the excimer laser and Stokes beams over the entire length of the probe oven. A portion of the probe beam was split off with a Suprasil flat and sent through a 1 m GCA/McPherson monochromator with an optical multichannel analyzer to facilitate tuning the probe beam. Ultimately the probe was detected with an EMI 955BQ photomultiplier tube (PMT) whose RC time was chosen to be more than ten times shorter than the decay time of observed signals. Output from the detector was displayed on an oscilloscope and digitized by a Biomation 610/Nicolet 1072 signal averaging system, which was triggered by the same pulse that triggered the excimer laser. Typically 128 shots were averaged before plotting on an X-Y plotter. Data were ultimately analyzed

by redigitizing the X-Y plots with a Hewlett Packard desktop calculator and digitally extracting a rate constant from each plot.

Once all equipment became operational, several days of data could be taken before a catastrophic failure occurred. On a successful day, UV probe radiation was detected immediately after warmup of the visible lasers; it was then tuned to the appropriate frequency using the OMA. Just before an experiment began the dye laser was tuned so that 90% of the probe beam was absorbed in the probe oven by the Pb resonance line at 266.3 nm for the $^3P_2$ level or at 261.4 nm for the $^3P_1$ level. This insured that small changes in the population of the metastable level could be detected and that the PMT was not saturated. The dye laser could be tuned manually between excimer laser shots to insure the 90% absorption figure. Usually the dye laser remained on the same longitudinal mode during the two minutes required to complete the accumulation of signals. After signals had been accumulated, the probe beam was blocked and the process was repeated to provide a baseline for future calculations. Before and immediately after the accumulations, the temperature of the probe oven tube was measured. If the two measurements did not agree to within 3^oC, the run was discarded. At least 30 minutes was allowed between experiments to allow the Pb vapor density to equilibrate after a temperature or buffer gas pressure change.

Several problems were overcome in the course of the experiments. It was found that liquid lead dissolves stainless steel at temperatures exceeding 1200^oC. For this reason, ceramic tubes were employed extensively, but the wicks eventually failed. Thermocouple metals met a fate similar to stainless steel, and repeatedly failed despite many efforts to shield them in various ways. Small dark deposits formed on the inside surfaces of the tube windows where the excimer laser beam passed. These deposits could not be totally removed, even with concentrated nitric acid, and eventually the windows had to be replaced. Extensive rf shielding of the excimer laser was necessary to prevent stray fields from perturbing the piezoelectric elements in the dye laser cavity and producing spurious signals. Two Ar^+ tube failures slowed progress considerably.

Helium used as buffer gas was USN grade. Argon was obtained from Matheson Gas Products with a stated purity of > 99.995%. Certified ACS grade Pb metal was obtained from Fisher Scientific Company and used without purification.

Rhodamine 590 tetrafluorborate and Rhodamine 560 chloride from Exciton Chemical Co. were used for several months each without degredation.

III. RESULTS

Transient signals of the quality shown in Fig. 3a were routinely recovered while probing the $6p^2\ ^3P_2 \leftarrow 6p7s\ ^3P_2$ absorption line at 266.3 nm. Figure 3 shows a record of the transmitted probe intensity as a function of time; the base line trace indicates that a small amount of pump light reached the detector but no other spurious effects occurred without the probe present. The rise and fall times of the pump light pulse are limited by the PMT RC times. When the probe was tuned far from resonance, or when the first oven was cooled so that no 459 nm pump was produced, no signal was observed on this resonance line, indicating that the Raman process was directly populating the $^3P_2$ level.

Since the signal represents the time resolved transmitted intensity I(t) through an optically thick sample,

$$I(t) = I_0 \exp\ \{-\alpha\ [Pb^*(t)]\} \tag{1}$$

where $[Pb^*(t)]$ is the time dependent concentration of Pb metastables, α is an appropriate extinction coefficient and ℓ is the sample length. If $[Pb^*(t)]$ decays exponentially from its value $\delta[Pb^*] + [Pb^*]_\infty$ at t=0 to its equilibrium value $[Pb^*]_\infty$ then we have:

$$I(t) = I_0 \exp\ \{-\alpha\ell(\delta[Pb^*] \exp(-kt) + [Pb^*]_\infty)\} \tag{2}$$

The decay constant k in the above equation can be obtained from the slope of the second logarithm of the recorded signal I(t),

$$A(t) \equiv \ln\left(-\ln \frac{I(t)}{[I(\infty)]}\right) \tag{3}$$

$$= -kt + \text{constant}$$

This procedure worked well in previous work,[14] and can be seen graphically in Fig. 3b.

To insure that the apparent metastable lifetimes were not determined by diffusion out of the probe beam, the buffer gas pressure was increased while keeping the temperature (hence [Pb]) constant. As can be seen in Fig. 4, the observed quenching rate appears to be only weakly dependent on buffer pressure. With beam diameters smaller than those used here, however, dramatic

effects were observed at low buffer gas pressures. A number of data were collected for each metastable level at various temperatures and buffer pressures. These are displayed in Fig. 5. From a least squares fit to these lines, quenching rate constants of $2.0 \pm .1 \times 10^{-13}$ cm^3 sec^{-1} for $^3P_1$ and $3.2 \pm .1 \times 10^{-13}$ cm^3 sec^{-1} for $^3P_2$ were calculated. The error bars are 3σ or 97% confidence values returned by the least squares program.

It was also noted that strong signals were observed on the $^3P_1$ resonance line using the excimer laser pump only. The signals disappeared when the 308 nm pump, the probe beam, or the Pb in the probe cell was removed. Tuning the probe off resonance also produced a null signal. Signals recovered with the 308 nm pump only were compared to those taken with both the 308 nm and 459 nm pumps. The only observed difference was a slight drop in the signal strength when two colors of pump were used and $^3P_1$ was monitored. Apparently a population of $^3P_1$ metastables was created by the excimer light alone. This effect will be discussed in greater detail below.

IV. DISCUSSION

By far the greatest experimental uncertainty arises in the calculation of the lead atom density. Some instrumental uncertainty in the temperature measurements was introduced by the optical pyrometer, even though the temperature readings were adjusted with well known formulas[15,16] to account for experimental technique. These adjustments amounted to approximately $+8^oC$ at 1200^oC corresponding to an increase in the calculated value of [Pb] by about 10%. If we assume that the instrumental accuracy is of this order, then the determination of the rate constant must be uncertain to the same degree. The 3σ values quoted above do not reflect this possible source of systematic uncertainty, because we have no other way to determine [Pb] more accurately.

The assumption that the Pb vapor reached its equilibrium pressure at the wall temperature is difficult to test experimentally. Reasonably good reproducibility was observed in signals taken at the same temperature but on different days. No appreciable change in baseline absorption occurred during the 10 minutes immediately preceding an experiment, indicating that an equilibrium had been reached. In the absence of cogent arguments to the contrary, we must assume that the Pb vapor pressure data of Ref. 12 gives the best approximation to the true Pb density.

As can be seen in Table 1, the quenching rate constants obtained here are faster than inert gas quenchers but slower than reactive partners, such as O_2 or CO, or partners where E→V energy transfer is expected,[5] such as N_2. This can be rationalized in a qualitative way by pointing out the greater size and polarizability of Pb. The sequence of collision partners He, Ar, Xe, Pb increases both in "hard sphere" size and polarizability. This trend is reflected in the quenching rates in Table 1. As has been pointed out,[4] the larger polarizability implies a stronger attractive interaction at larger internuclear distances, thus utilizing dipole-induced dipole interactions at larger impact parameters. It would be interesting to compare the quenching rate by Pb to that of an atom of similar size and polarizability, such as Hg, where resonant effects providing alternate, efficient pathways, such as E→E energy transfer, are not operating.

A least squares analysis of Fig. 4 renders a value of 5-7 x 10^{-16} cm^3 sec^{-1} for the quenching of either metastable by Ar. This value is in fair agreement with other reported values[3,4] for the relaxation of the $^3P_1$ level by Ar, and is somewhat slower than the values for the $^3P_2$ state. It is possible that an impurity which quenches $^3P_2$ selectivity was introduced with the Ar buffer in a previous work; Trainor and Ewing[5] felt that the culprit was H_2O when they observed a similar effect when working with Xe. Unfortunately, no quenching rate constants of $^3P_2$ by H_2O have been reported. Because these rate constants are so small, we cannot be sure that some impurity in the Ar supply is not limiting observed quenching rate, hence the values in Table 1 are upper bounds as noted.

Elucidating the mechanism of quenching the metastables by Pb requires some speculation. Energy pooling, such as

$$Pb^* + Pb^* \rightarrow Pb^{**} + Pb \qquad (4)$$

can be ruled out because the increase in metastable population induced by the pump lasers is only a few percent of the background thermal population, which is at most 10^{-4} of the ground state density. Three-body collisions to form dimers,

$$\begin{aligned} Pb(^3P_0) + Pb(^3P_{1,2}) + M &\rightarrow Pb_2^* + M \\ &\rightarrow Pb_2 + M \end{aligned} \qquad (5)$$

seem unlikely in view of the insensitivity of the quenching rate to large

buffer gas pressures. This points to direct deexcitation of the metastables by ground state atoms.

If the eigenstates for lead dimer, Pb_2, were well known, a mechanism might be proposed whereby the colliding ground state and metastable atoms exit from the collision along a repulsive potential leading to two ground state atoms. Unfortunately, spectroscopic data[17,18,19] do not include dimer states arising from the $^3P_0 + {}^3P_{1,2}$ atomic combinations. The existence of a few repulsive states was deduced[18] but none of these would produce atoms in any of the $6p^2$ spin-orbit configurations. We are left with the need to postulate that such states are available, but can say no more about them than that they must cross within a few kT of the dissociation energy of the Pb_2 X (ground) state.

Another dilemma is posed by the production of $^3P_1$ and not $^3P_2$ atoms by the 308 nm pump alone. Spontaneous Raman scattering would preferentially[20] produce $^3P_2$ atoms and can therefore be ruled out. Dissociation of dimers, which are present[21] in mole fractions of approximately 10^{-4} at these temperatures may be accomplished with the absorption of a single photon per molecule. Since the spectroscopy of Pb dimers is so poorly known, the reason why absorption would occur preferentially to a predissociating level which produces $^3P_1$ atoms remains a speculation. The observation above that the absolute amount of $^3P_1$ metastables produced is decreased when the 308 nm pump power is decreased, that is, when the 308 nm pump is depleted by SRS to form the 459 nm pump, is consistent with this argument of making $^3P_1$ directly with the 308 nm pump.

In the case that both 308 and 459 nm pumps were used while probing the $^3P_1$ state, it is not possible to determine the extent to which the $^3P_2$ population produced by SRS relaxes into the $^3P_1$ state enroute to the ground state. Since the decay rates of the metastable levels are very similar, any relaxation to $^3P_1$ from $^3P_2$ would be indistinguishable in its temporal behavior from the $^3P_1$ population initially created by the pump pulse directly. In fact, the amplitude of signal on the $^3P_1$ resonance line created by stepwise relaxation of $^3P_2$ metastables would be very small, since the relaxation rates of the two states are so close. Thus our results do not contain enough information to make an estimate of the branching ratio of rates $^3P_2 \rightarrow {}^3P_1$ and $^3P_2 \rightarrow {}^3P_0$, which presumably[4] favors the stepwise process $J=2 \rightarrow 1 \rightarrow 0$.

Using the Pb quenching rates obtained here, we can estimate the ultimate repetition rate of a Pb vapor Raman cell. At a typical operating temperature

of 1100°C, the quenching rate would be approximately 1×10^{-4}, implying that pulse rates of 1-10 kHz could be sustained provided that the cell was cleverly designed to suppress resonant acoustic disturbances of the medium. Since presently envisioned devices[10] for undersea communication require a < 1 kHz repetition rate, the Pb Raman converter would not limit the overall system in this respect.

ACKNOWLEDGEMENT

We wish to thank Mr. Thomas McClelland for expert technical assistance and Dr. B. L. Wexler for helpful discussions.

References

1. K.H.L. Erhard and R.G.W. Norrish, Proc. Royal Soc. A, 234, 178 (1956).
2. K.H.L. Erhard and R.G.W. Norrish, Proc. Royal Soc. A, 259, 297 (1961).
3. D. Husein and J.G.F. Littler, Int. J. Chem. Kin. 6, 61 (1974).
4. J.J. Ewing, D.W. Trainor and S. Yatsiv, J. Chem. Phys. 61, 4433 (1974).
5. D.W. Trainor and J.J. Ewing, J. Chem. Phys. 64, 222 (1976).
6. W.T. Silfvast, L.H. Szeto and O.R. Wood, II, Appl. Phys. Lett. 36, 615 (1980).
7. L. Fu-Cheng, Opt. Commun. 36, 387 (1981).
8. R. Burnham and N. Djeu, Opt. Lett. 3, 215 (1978).
9. N. Djeu, Appl. Phys. Lett. 35, 663 (1979).
10. R. Burnham and E.J. Schimitschek, Laser Focus 17, 54 (1981).
11. R. Burnham, Opt. Commun. 24, 161 (1978).
12. D.H. Shiu and Z.A. Munor, Metallurgical Trans. 2, 2953 (1971).
13. B.L. Wexler, B.E. Wilcomb and N. Djeu, J. Opt. Soc. Am. 70, 863 (1980).
14. J.D. Eversole and N. Djeu, J. Chem. Phys. 71, 148 (1979).
15. J. Volmer, J. Opt. Soc. Am. 47, 926 (1957).
16. H.J. Kostkowsky and R.D. Lee, "Theory and Methods of Optical Pyrometry," NBS Monograph 41 (1962).
17. E.N. Shawhan, Phys. Rev. 48, 343 (1935).
18. S. Weniger, J. Physique 38, 595 (1967).
19. R.A. Teichman, III and E.R. Nixon, J. Mol. Spec. 59, 299 (1976).
20. N.P. Penkin and Yu. Yu. Slavenas, Opt. Spectry 15, 83 (1963).
21. D.R. Stull and H. Prophet, "JANAF Thermochemical Tables," 2nd ed., Nat. Stand. Ref. Data Ser., NBS 37 (U.S. Govt. Printing Office, Wash., D.C., June 1971).

TABLE 1. Quenching rate constants of Pb metastables, in cc/sec

Partner/State	$^3P_1$	$^3P_2$	Ref.
He	1.1×10^{-16}	$<1.3 \times 10^{-17}$	3
Ar	1×10^{-16}	2×10^{-15}	3
	$<2.3 \times 10^{-16}$	$<2.0 \times 10^{-15}$	4
	$<5.6 \times 10^{-16}$	$<7.4 \times 10^{-16}$	This work
Xe	$<6 \times 10^{-16}$	$<3 \times 10^{-15}$	4,5
Pb	2.0×10^{-13}	3.2×10^{-13}	This work

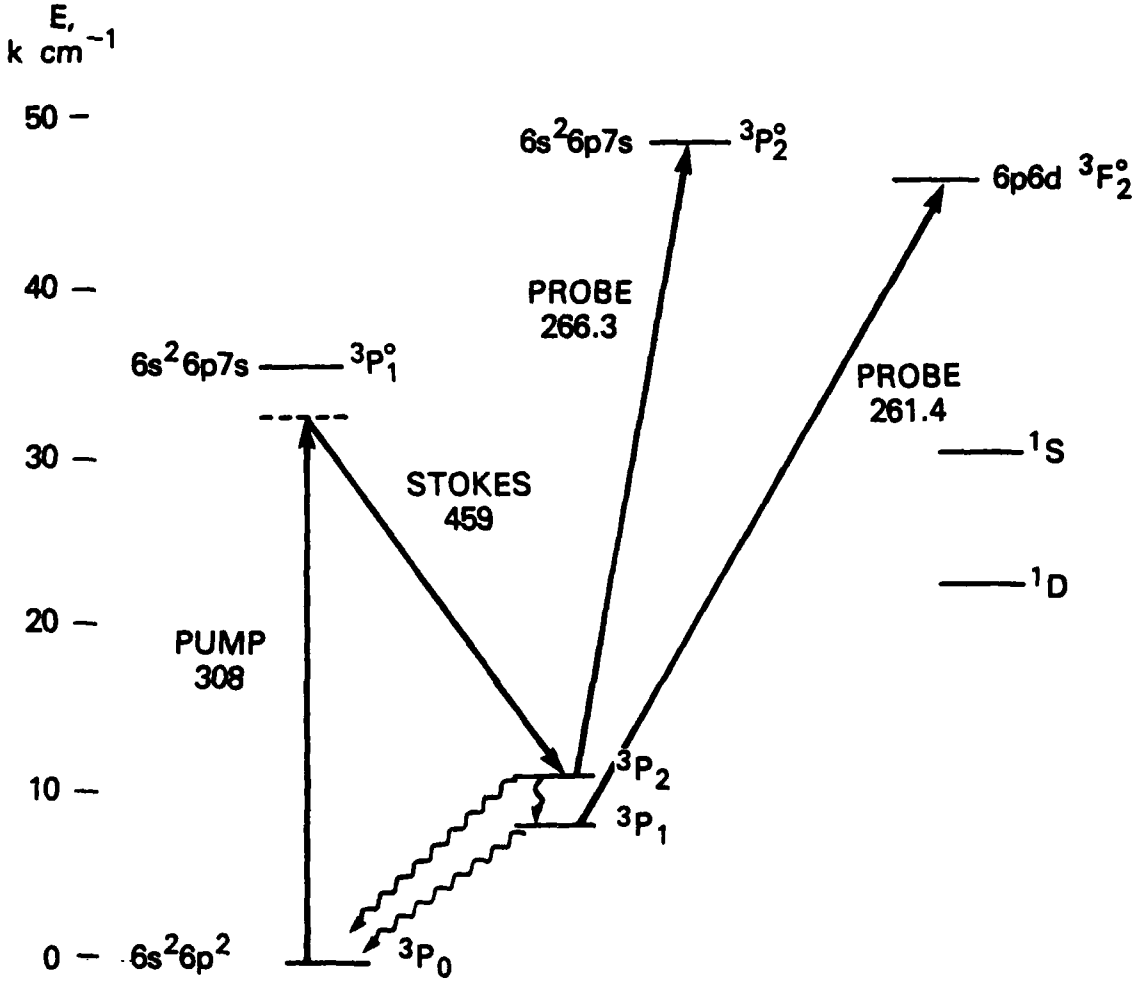

Fig. 1 - Grotrian diagram for PbI, showing SRS by XeCl laser pump and probing transitions for two metastable states

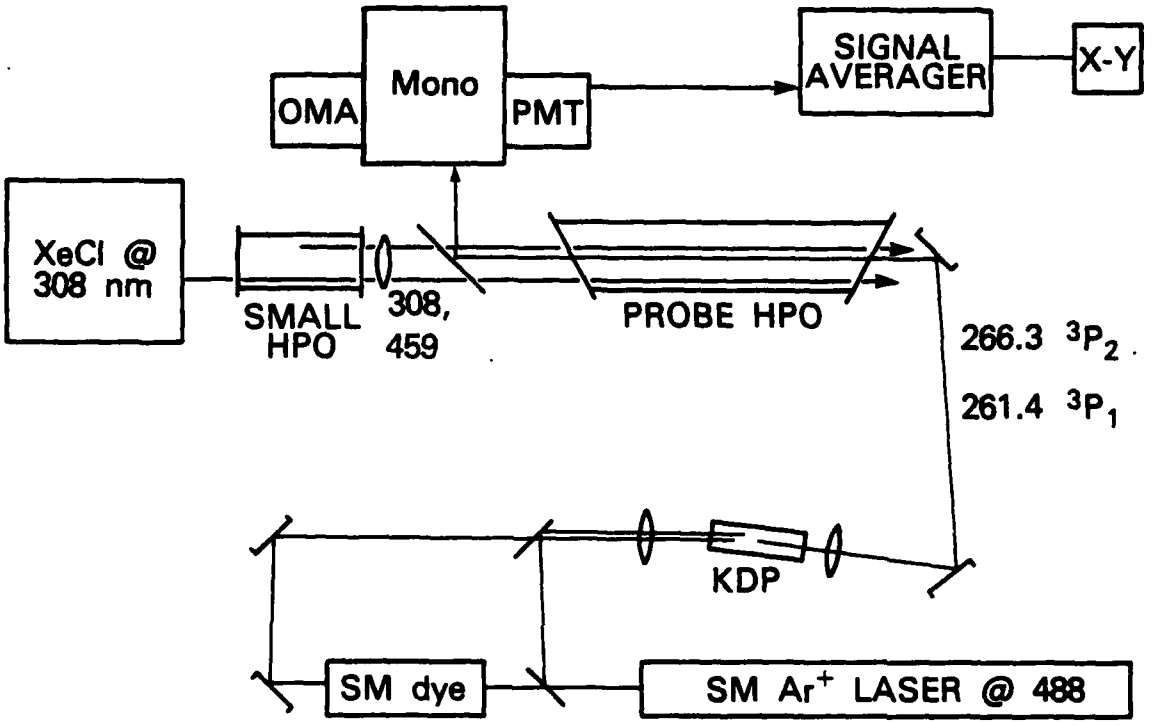

Fig. 2 - Apparatus for producing and detecting Pb metastables. HPO - heat pipe oven; SM - single mode laser; Mono - 1 m monochromator; OMA - optical multichannel analyzer; PMT - photomultiplier tube.

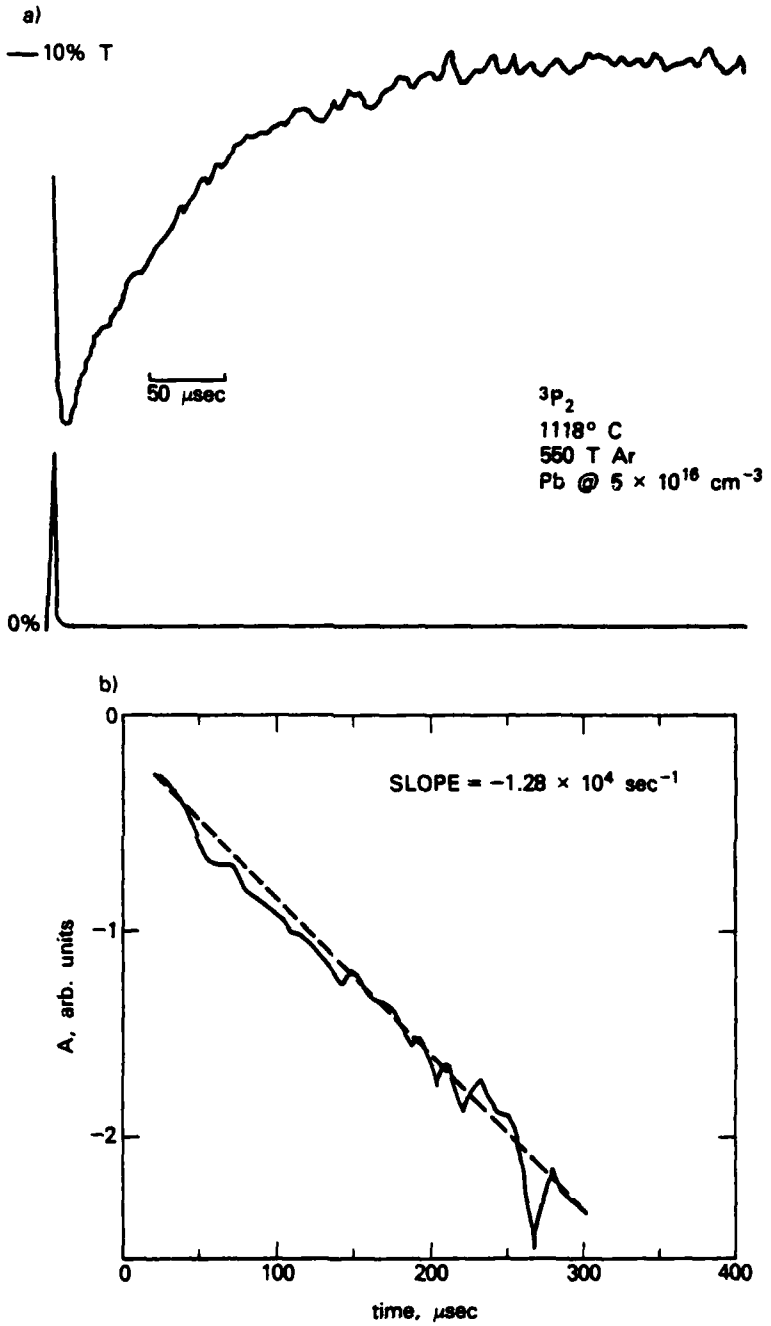

Fig. 3 - (a) Typical signal recovered after accumulating 128 transients. The top trace shows transient absorption (downward deflection) slightly off line center; bottom trace was recovered by blocking the probe beam; (b) plot of second logarithm, A, vs. time (see Eqn. 3), showing least squares line (dashed).

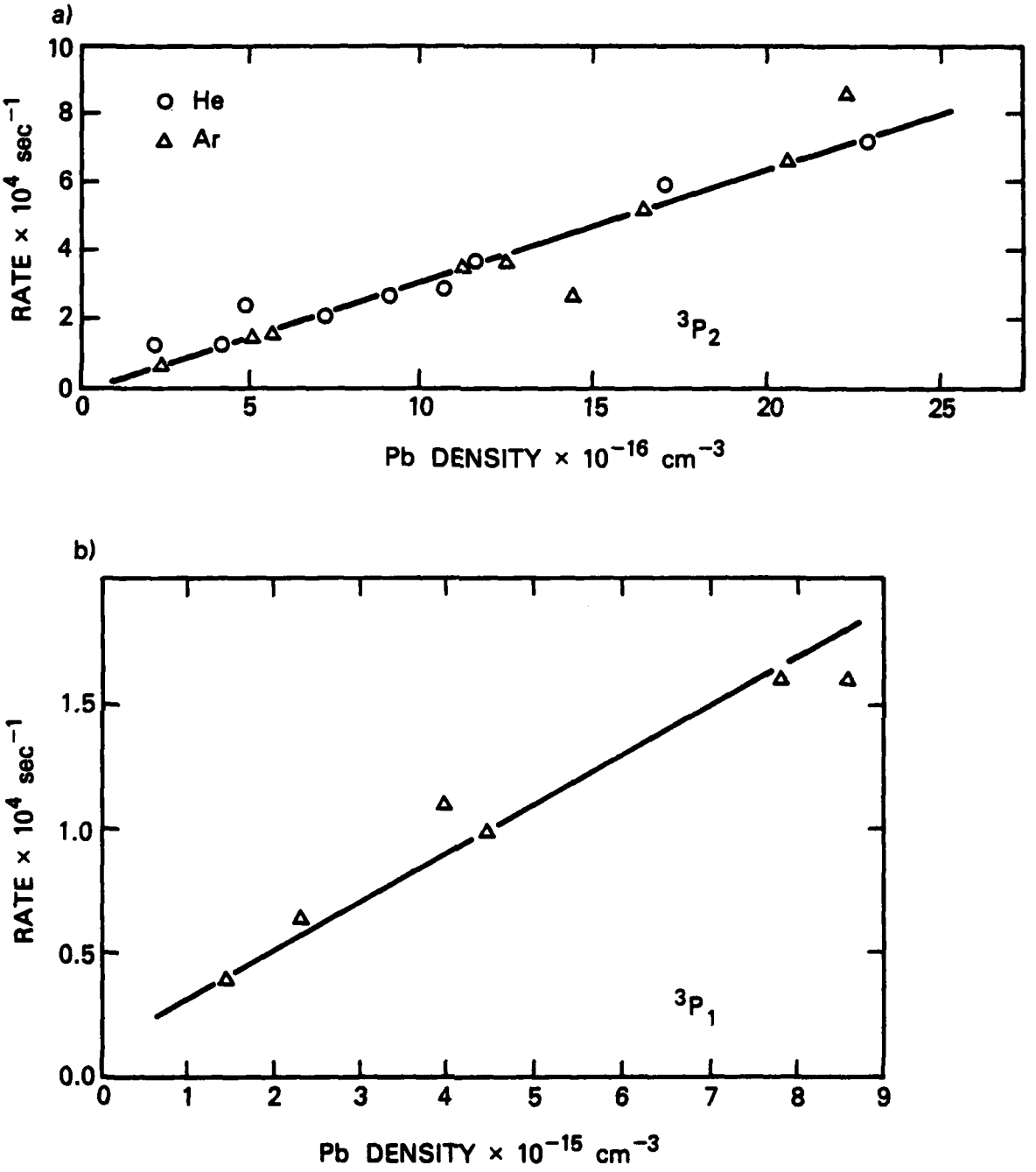

Fig. 4 - Observed quenching rate vs. Ar buffer pressure. Least squares slopes are 5.6×10^{-16} cc/sec for $^3P_1$ and 7.4×10^{-16} cc/sec for $^3P_2$.

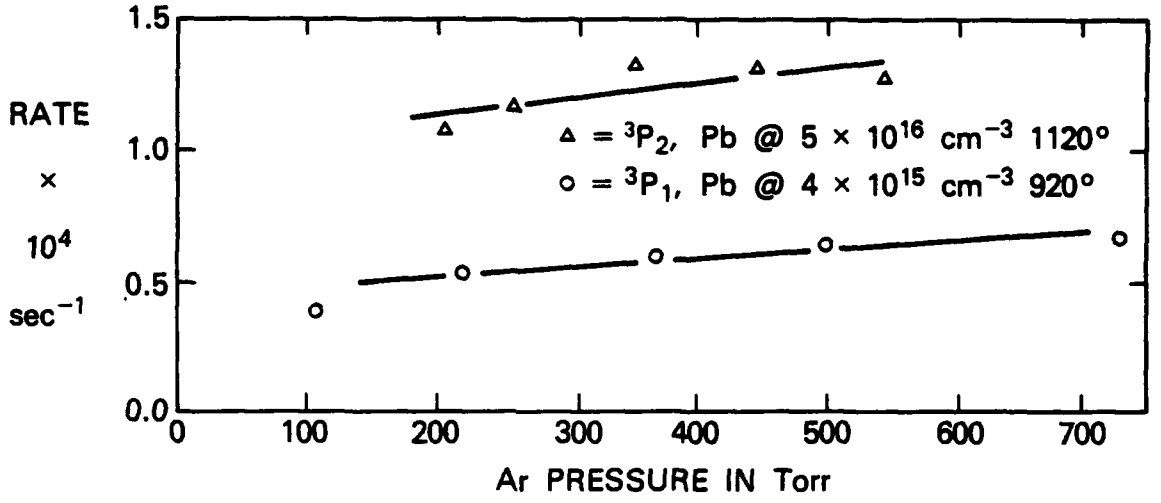

Fig. 5 - Observed pseudo-first-order quenching rates vs. [Pb] for (a) $^3P_2$ and (b) $^3P_1$.